REVIEW SUMMARY

OPTOELECTRONICS

Optoelectronic metadevices

Son Tung Ha†, Qitong Li†, Joel K. W. Yang, Hilmi Volkan Demir, Mark L. Brongersma*, Arseniy I. Kuznetsov*

BACKGROUND: Metasurfaces, thin planar arrays of subwavelength nanostructures, have transformed the way we can control the flow of light. Recent breakthroughs have extended their capabilities beyond passive manipulation, allowing dynamic control of light emission, absorption, and modulation. By fusing metasurfaces with optoelectronic devices, such as light-emitting diodes (LEDs), lasers, modulators, and photodetectors, metadevices are emerging that offer critical performance improvements and entirely new functionalities. These bring exciting opportunities in applications such as augmented reality (AR) and virtual reality (VR) systems, optical communication, smart thermal management, computational imaging, solar energy harvesting, and quantum technologies. As metasurface technology matures, its integration with optoelectronics is expected to play an increasingly prominent role in the evolution of advanced optoelectronic devices.

ADVANCES: Here, we discuss the recent progress, emerging opportunities, and ongoing challenges in integrating metasurfaces into optoelectronic devices. By judiciously patterning the metallic, semiconducting, and insulating layers inside conventional optoelectronic devices into nanostructures, we can capitalize on their optical resonances to improve performance. It is also opening an unexpected new opportunity, in which nanostructures in a device can simultaneously perform important optical, electronic, mechanical, and thermal functions. We explore how these notions can be applied to realize conceptually new optoelectronic devices for light emission, modulation, and detection.

In LEDs, metasurfaces have been used to enhance the radiative decay of emitters, leading to higher quantum yields and longer device lifetimes. The ability to tailor the outcoupling of certain optical channels further facilitates directionality, spectral, and polarization control, and improves extraction efficiency. Metasurface-enhanced lasers enrich cavity design principles and broaden the landscape of accessible physics. Notable improvements have already been demonstrated in beam quality, emission control, and polarization selectivity. These are critical for applications in optical communication, precision sensing, and computational imaging. Moreover, metasurfaces have been used in optical modulators to substantially enhance the generally weak electro-optic effects, enabling faster phase and amplitude modulation in a smaller footprint to facilitate higher spatial resolution for AR/VR, LIDAR (light detection and ranging), and holographic displays. Photodetectors have also benefited from metasurface integration. They can filter or selectively absorb photons in specific optical modes, thus capturing not only intensity but also complex light-field information, including the spectral, phase, and polarization characteristics of incident light. This capability has led to advances in imaging systems, particularly in hardware-based image processing and optical computing. Furthermore, metasurfaces can be patterned on top of ultrathin, flexible solar cells to improve their power conversion efficiency by delivering valuable antireflection and light-trapping functions.

OUTLOOK: The integration of metasurfaces into optoelectronic devices holds considerable promise for advancing technology by enabling ultracompact, efficient, and multifunctional systems. However, to fully realize this promise, a codesign approach is crucial, ensuring that both photonic and electronic functionalities are optimized in tandem. Achieving a balance between nanoscale light control and efficient electronic operation, such as charge injection and thermal management, remains a challenge. The design of metadevices must consider material compatibility and the strategic placement of metasurfaces relative to active electronic layers. Additionally, large-scale fabrication techniques compatible with industry standards are essential for transitioning these technologies to commercial applications. As the field progresses, interdisciplinary collaboration between photonic, electronic, materials science, and manufacturing will be key to overcoming these challenges and unlocking the full potential of metasurface-based optoelectronic devices for practical applications. ■

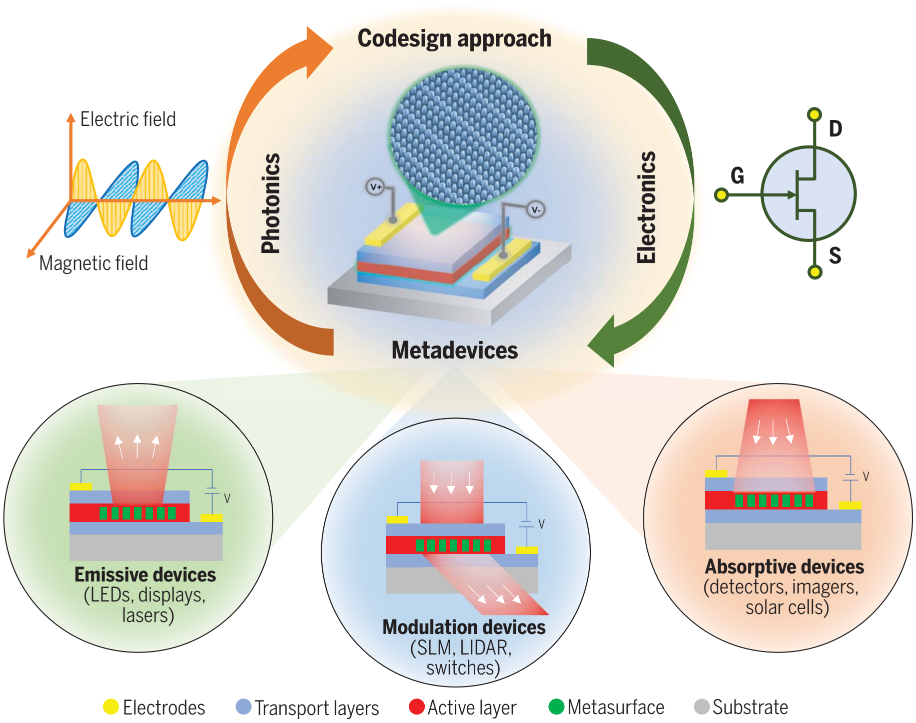

Optoelectronic metadevices. The effective integration of metasurfaces into electronic devices demands a careful codesign approach that addresses both photonic and electronic components. Depending on their functionality, metadevices can be categorized into three types: (i) emission devices (LEDs, displays, lasers); (ii) modulation devices (spatial light modulators, LIDAR, switches); and (iii) absorptive devices (detectors, imagers, solar cells).

The list of author affiliations is available in the full article online.
*Corresponding author. Email: brongersma@stanford.edu (M.L.B); arseniy_kuznetsov@imre.a-star.edu.sg (A.I.K)
†These authors contributed equally to this work.
Cite this article as S. T. Ha *et al.*, *Science* **386**, eadm7442 (2024). DOI: 10.1126/science.adm7442

READ THE FULL ARTICLE AT
https://doi.org/10.1126/science.adm7442

REVIEW

OPTOELECTRONICS

Optoelectronic metadevices

Son Tung Ha[1]†, Qitong Li[2]†‡§, Joel K. W. Yang[3], Hilmi Volkan Demir[4,5], Mark L. Brongersma[2]*, Arseniy I. Kuznetsov[1]*

Metasurfaces have introduced new opportunities in photonic design by offering unprecedented, nanoscale control over optical wavefronts. These artificially structured layers have largely been used to passively manipulate the flow of light by controlling its phase, amplitude, and polarization. However, they can also dynamically modulate these quantities and manipulate fundamental light absorption and emission processes. These valuable traits can extend their application domain to chipscale optoelectronics and conceptually new optical sources, displays, spatial light modulators, photodetectors, solar cells, and imaging systems. New opportunities and challenges have also emerged in the materials and device integration with existing technologies. This Review aims to consolidate the current research landscape and provide perspectives on metasurface capabilities specific to optoelectronic devices, giving new direction to future research and development efforts in academia and industry.

Metasurfaces are planar optical elements composed of dense arrays of subwavelength nanostructures. Their desirable form factor and ability to deliver a myriad of optical functions make them very attractive for a wide range of technologies. Thus far, they have primarily been used to control the flow of light by capitalizing on the light-scattering properties of the nanostructures. Here, their function is to passively transform one optical wavefront into another. However, there is an equally large opportunity to integrate metasurfaces directly into optoelectronic devices to control the emission, modulation or manipulation, and detection of light. For example, metasurfaces can be integrated with light sources to realize large enhancements in radiative decay rates (i.e., Purcell effect) or to achieve new ways of dynamically controlling the angular and polarization properties of emitted light fields by, e.g., patterning nanoscale electrodes. By merging nanoelectronics and metasurface technology, it is possible to create active metasurfaces capable of dynamically shaping optical wavefronts and to deliver new designs for beam steering [e.g., for light detection and ranging (LIDAR)] and optical sensing platforms. Metasurfaces can also be embedded into photodetectors to realize never-before-seen functionalities. Here, one can engineer optical fields inside metasurfaces to enhance the absorption efficiency for specific light waves of interest and open the door to new photodetectors, solar cells, and computational imaging functions.

Integrating metasurface concepts into optoelectronic devices is an essential step toward the commercialization of this technology. Although the promise of densely integrating planar electronics with planar metasurfaces into ultracompact device platforms is evident, it faces a number of challenges for practical implementation. These challenges include scalable fabrication techniques, material compatibility, the need for careful codesign of the optics and electronics, and system-level integration. Addressing these issues is crucial to unleash the full potential of metasurfaces and ensure their widespread adoption.

In this paper, we will give an overview of the state-of-the-art metasurface-based optoelectronic devices, highlighting key achievements, underlying principles, and technological challenges. We also discuss various strategies used for metasurface fabrication, materials selection, codesign with electronics, and device integration while exploring potential avenues for future research and development. By consolidating the existing knowledge and identifying the current obstacles, this Review aims to provide researchers, engineers, and industry professionals with a roadmap toward successful commercialization of integrated metasurface technologies.

[1]Institute of Materials Research and Engineering (IMRE), Agency for Science, Technology and Research (A*STAR), Singapore. [2]Geballe Laboratory for Advanced Materials, Stanford University, Stanford, CA, USA. [3]Engineering Product Development, Singapore University of Technology and Design, Singapore. [4]LUMINOUS! Center of Excellence for Semiconductor Lighting and Displays, The Photonics Institute, School of Electrical and Electronic Engineering, School of Physical and Mathematical Sciences, School of Materials Science and Engineering, Nanyang Technological University, Singapore. [5]UNAM—Institute of Materials Science and Nanotechnology, The National Nanotechnology Research Center, Department of Electrical and Electronics Engineering, Department of Physics, Bilkent University, Bilkent, Ankara, Turkey.
*Corresponding author. Email: brongersma@stanford.edu (M.L.B); arseniy_kuznetsov@imre.a-star.edu.sg (A.I.K)
†These authors contributed equally to this work.
‡Present address: Department of Applied Physics, Stanford, CA, USA.
§Present address: SLAC National Accelerator Laboratory, Menlo Park, CA, USA.

Codesign opportunities in nanoscale optoelectronic devices

The scaling of optoelectronic devices has come with many important benefits. Most notably, it has brought opportunities to reduce the power consumption of information processing and communication systems. Such systems now consume ~10% of the worldwide electricity production. The rapid developments in artificial intelligence and machine learning are projecting even higher energy requirements with a nonsustainable impact on greenhouse gas emissions (1–3). At the nanoscale, a number of beneficial physical effects naturally become available, including quantum-mechanical effects and optical resonances that can deliver extreme light–matter interaction (4, 5). By judiciously structuring devices to capitalize on these effects, it is possible to gain markedly improved control over the flow of charge and light to create new functionalities and achieve reductions in power consumption that go well beyond those expected from basic scaling rules.

The fabrication tools that have enabled the scaling in the semiconductor industry can also create high-performance optoelectronic devices and circuits in which semiconductors, dielectrics, and metals are interwoven at the nanoscale. Their assembly does not simply follow the same design rules as larger-scale optoelectronic systems, and new design concepts can be harnessed to effectively leverage the strengths of each constituent and to capitalize on the benefits of dense, chip-scale integration. To illustrate these points, we analyze a number of nanostructured devices for light emission, modulation, and photodetection and emphasize opportunities that can enable radically improved system architectures that combine electronics and photonics together in a seamless, highly-integrated fashion. Figure 1 shows the summary of the most important optoelectronics metadevices, their typical device configurations, materials, and functionalities enabled by metasurfaces. Our examples highlight that in nanoscale optoelectronic systems, the exact boundaries between optical, electronic, mechanical, and thermal elements are often blurred, and many components can perform multiple functions simultaneously. This is very different from current large-scale systems, including state-of-the-art miniaturized devices, such as smartphone cameras, in which the optical elements (e.g., lenses and color filters for imaging), electronics (e.g., photodetection and image processing), mechanics (e.g., zoom and image stabilization systems), and thermal elements (e.g., cooling) are all easily identified and spatially separated.

We will start by analyzing the multiple roles that metallic structures can play in nanostructured optoelectronic devices. Metals serve an important role as high-conductivity electrodes for injecting and extracting charges and applying

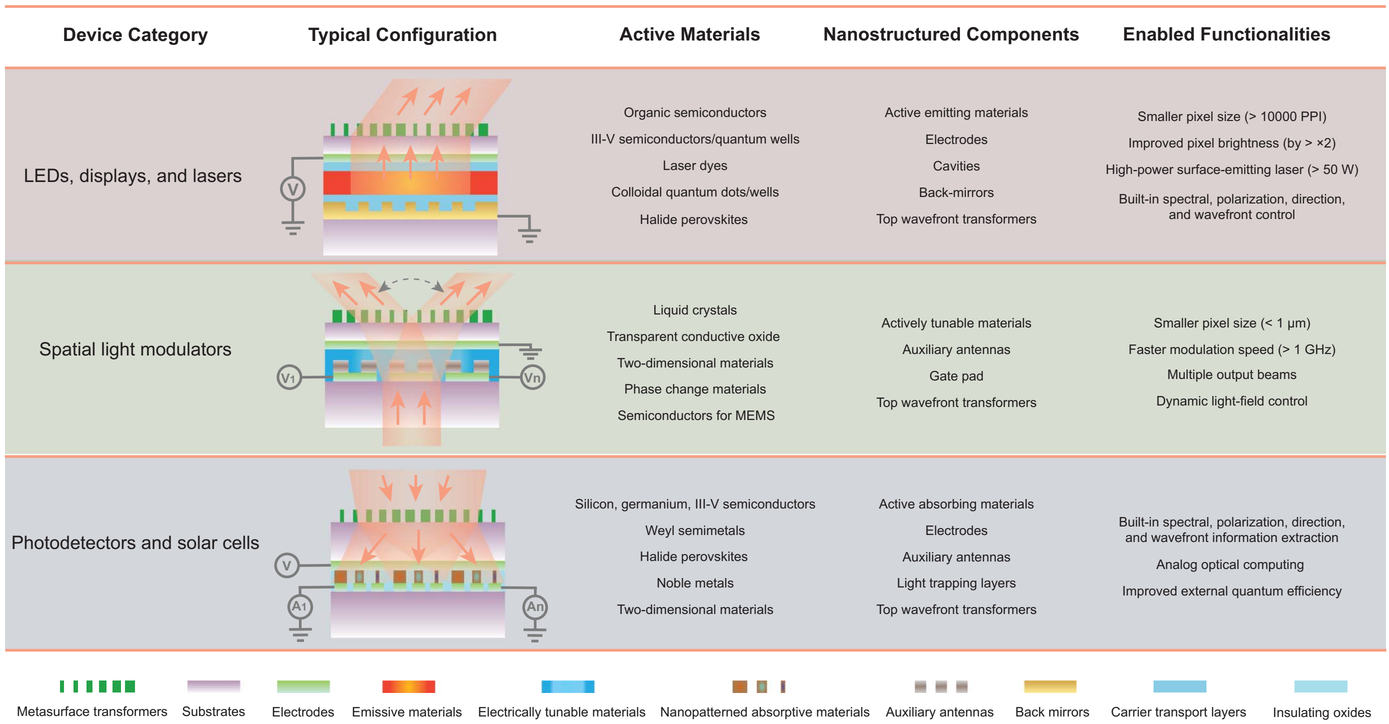

Fig. 1. Summary of different types of optoelectronic metadevices and enabled functionalities.

electric fields capable of modulating or tuning optical materials' properties. In addition to these electronic functions, nanopatterned metals can also be used in optical roles as light reflectors (*6*, *7*), plasmonic resonators and waveguides (*8*, *9*), or optical antennas (*10*, *11*), capable of enhancing and controlling light-matter interaction. These optical functions need to be carefully optimized while not negatively affecting the electronic performance.

We first analyze the benefits of electronic and optical codesign for a simple, planar metallic electrode in an optoelectronic device that is patterned into a metasurface mirror. At first sight, it may seem that there is not much to optimize for a metallic mirror beyond its reflectance. However, in an optoelectronic device composed of multiple thin layers, the reflection phase is at least as important as reflection amplitude because it governs the spatial location of the nodes and antinodes in the standing wave pattern in the electric field intensity (*7*, *12*, *13*). To achieve strong interaction with active absorber, modulation, or emitter layers, it is critical to align the maxima in the electric field strength with the position of these layers. However, often the use of high-conductivity, smooth metallic electrodes can cause unwanted effects as they produce a π-phase reversal for reflected light waves, creating a standing wave with an undesired, reduced light intensity near the reflective surface. To achieve strong light–matter interaction with a thin active layer, they need to be spaced approximately one-quarter wavelength away from the metal, and this may limit the charge injection or extraction (*14*, *15*). This challenge can be circumvented by using a nanopatterned metamirror, as shown in Fig. 2A (*7*), whose reflection phase ($\varphi = \pi$) is tunable from that of a perfect electric mirror to a perfect magnetic mirror ($\varphi = 0$). This tunability in the reflection phase can also be exploited to ensure operation near a Fabry-Pérot resonance in a layered device. To benefit from such optical resonances, the roundtrip phase for light in the device needs to equal an integer number of 2π. Typically the roundtrip phase is tuned with the mirror spacing, but metamirrors can generate any desired reflection phase across the 0 to 2π range, as shown in Fig. 2B (*7*). This leaves the mirror spacing as a free parameter that can be optimized on the basis of other considerations, e.g., electronic, fabrication ease, ideal materials choice, etc. Control over the antinode positions and resonances can lead to notable enhancements in light absorption in thin photodetection and solar energy–harvesting systems (*7*).

Besides engineering the reflection phase, nanopatterned metallic mirrors can also control the excitation and propagation of surface plasmon polaritons at the metal surface. Figure 2C shows the beneficial use of a metamirror in modulators to enhance light–matter interaction with an ultrathin active layer (*9*). In this work, a metal electrode can electrically modulate the intensity of a reflected light beam by electrically switching exciton resonances on and off in a two-dimensional (2D) semiconductor. Therefore, the performance of this modulator critically relies on the presence of a strong excitonic material resonance. Excitons can offer extremely strong and high-speed optical modulation. However, such resonances severely weaken at room temperature, where nonradiative decay dominates the radiative one. The application of a periodic nanopattern to the metal surface brings the opportunity to grating couple incident, free-space photons to guided surface plasmons that notably enhance the light–matter interaction and also provide a favorable Purcell effect that boosts the radiative decay rate to such an extent that it can outpace the nonradiative decay at room temperature. Metallic-strip electrodes have also been used as plasmonic waveguides and as leads to apply fields in electro-optic modulators (*16*) or heating elements in thermo-optic modulators (*8*). In such designs, an outstanding overlap of the guided plasmon modes with the electrically driven active medium is guaranteed.

Optical antennas can control the emission from quantum emitters by modifying the local density of optical states via the Purcell effect. This can deliver control over the decay rate of quantum emitters as well as the directionality and polarization of the light emission. However, their implementation in optoelectronic devices has been hampered by the need to precisely place emitters near an antenna and to efficiently excite them electrically. This requirement can be circumvented with the help of antenna electrodes that facilitate simultaneous operation as electrodes for current injection and as antennas capable of optically

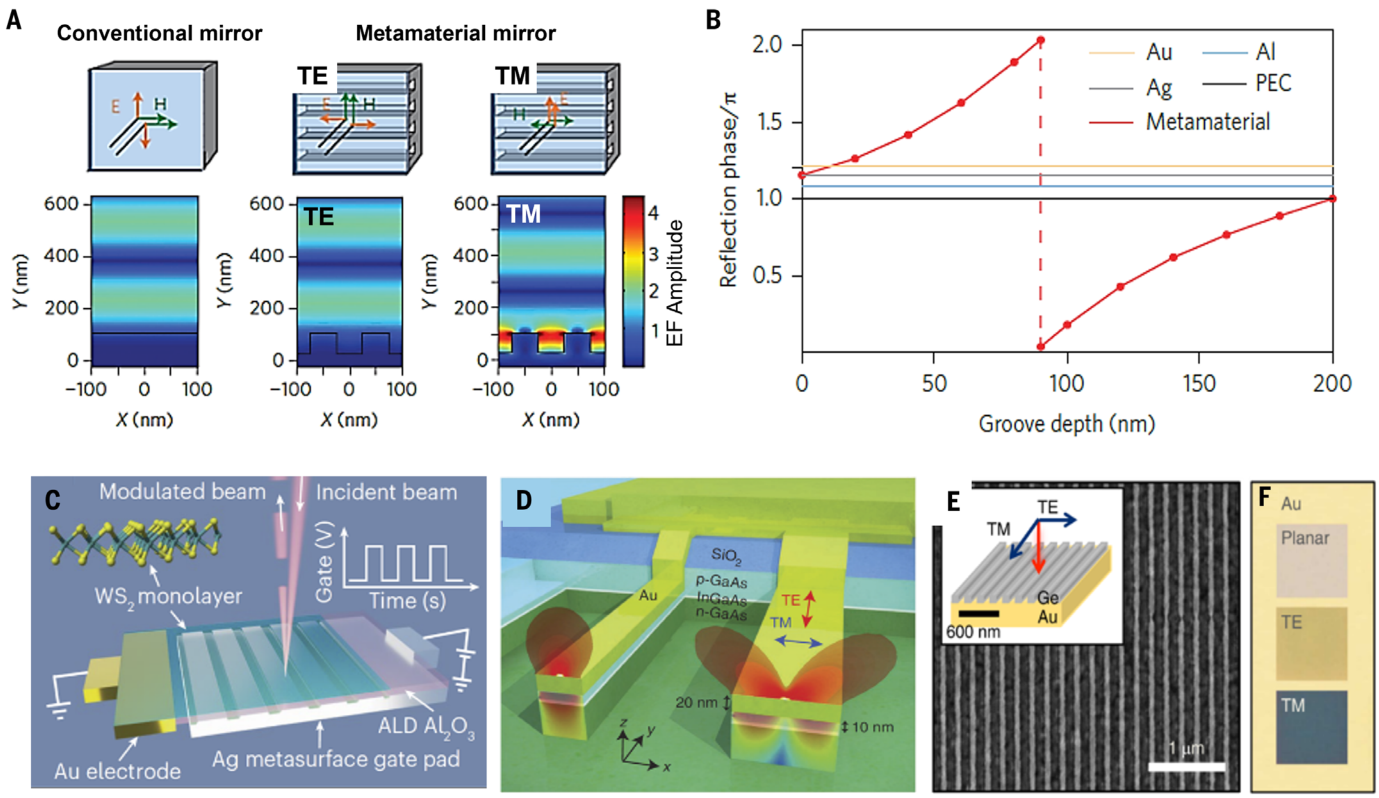

Fig. 2. Multiple roles of metallic and semiconductor nanostructures in optoelectronic devices. (**A**) Difference in the optical behavior of a conventional mirror and a metamirror. In transverse electric (TE) polarization, the metamirror behaves as a conventional electric mirror that flips the electric field of an incident light wave on reflection, whereas for transverse magnetic (TM) polarization, it serves as a magnetic mirror capable of flipping the magnetic field (*7*). (**B**) Dependence of reflection phase from a metamirror on the metal groove depth (wavelength 600 nm). The reflection phases for conventional metal reflectors are shown for comparison. PEC: perfect electrical conductor (*7*). (**C**) Schematic of a free-space optical modulator that capitalizes on the dynamically tunable exciton resonances supported by the atomically thin semiconductor WS_2 (*9*). A metal-oxide-semiconductor configuration is used to electrically gate the device. This can turn on and off the exciton resonances in the WS_2 and modulate the intensity of a reflected light beam. The nanopatterning of the metal electrode allows for the coupling to surface plasmons and an enhanced light–matter interaction. (**D**) Two Au electrodes of different widths can inject charge into a quantum well (QW) ridge. The electrodes also support distinct surface plasmon resonances that can be dipolar or quadrupolar in nature, depending on their width, as shown by the magnetic field amplitude maps within the semiconductor. When current is injected into the QW via the antenna electrodes and the substrate, light is emitted with an angular emission pattern and polarization that is characteristic of the electrode dimensions (*11*). (**E**) Top-view scanning electron microscope (SEM) image of a fabricated metafilm with a 200-nm period and 0.3-duty-cycle germanium (Ge) nanowires. The scale bar is 1 μm. Inset shows a schematic of the measurements (*19*). (**F**) White light reflection images taken from a thin 50-nm Ge film (top) and metafilms with 30-nm-wide beams under TE and TM illumination on an Au background.

manipulating the electroluminescence (*11*). Antenna electrodes naturally deliver electrically excited carriers to the vicinity of the antenna and maximize the optical coupling of the emission to a single, well-defined antenna mode (Fig. 2D).

Semiconductors also play vital roles in optoelectronic devices and there are distinct opportunities for structuring them into metasurfaces as well. These materials can efficiently convert optical signals to electronic signals via the generation of photoexcited carriers, and vice versa through the recombination of electrically injected carriers. The prominent electro-optic and carrier effects in semiconductors can also be harnessed to modulate their coherent interaction with light. Similar to metallic nanostructures, nanopatterned semiconductors also support strong optical resonances, termed Mie resonances (*5*), which endow them with improved and highly engineerable light emission, modulation, and absorption functions. On resonance, incident light waves can drive the bound charges in these highly polarizable, high-index structures into oscillation. This produces intensified light fields inside and around the structure that can be used in devices. For example, in a semiconductor nanowire photodetector (*17*), the Mie resonances open up ways to spectrally engineer and enhance light absorption. These benefits can also be translated to judiciously nanopatterned semiconductor metalayers. From the first systematic studies on structural colors on individual semiconductor nanostructures and metasurfaces (*18*), it became clear that the resonant behavior of the individual nanostructures could be encoded into metafilms assembled from these structures. By carefully choosing the sizes and spacings of nanostructures, near-unity light absorption can be achieved at one or more desired, target wavelengths (*19*). Figure 2, E and F, illustrate the impact of patterning a continuous germanium (Ge) film into a metafilm of densely spaced nanowires. Figure 2F shows the normal-incidence reflection images taken for transverse magnetic (TM) polarized light with the electric field parallel to the length of the nanowires and for the orthogonal transverse electric (TE) polarization. Here, the anisotropic nature of the building blocks leads to different optical responses. Notably, the removal of about two-thirds of the Ge film gives rise to a greatly enhanced absorption under TM illumination as the weak Fabry-Pérot resonance supported by the continuous Ge film is replaced by stronger Mie resonances of the nanowires.

The integration of resonant nanostructures into optoelectronic devices heralds a new era in which the miniaturization of devices does not come at the cost of performance, and instead, opens up avenues for innovation in areas such as solar energy harvesting, imaging systems, and secure communications. The potential impact and importance of metasurface-integrated devices lie in their ability to transform the landscape of technology, leading to smarter, more efficient, and highly adaptable optoelectronic applications. In the following sections, we will discuss the current progress and challenges for each type of metadevices shown in Fig. 1 in detail.

Light-emitting diodes and displays

In light-emitting diodes (LEDs), quantum emitters are electrically driven to produce light by spontaneous emission. These devices are engineered with a desire to make the emission efficient, while also controlling different attributes of the generated light. However, the set of these attributes and the extent to which they can be controlled are usually limited. Typically, the peak emission wavelength and emission linewidth are determined by the choice of emitters. However, the available options are often limited to semiconductor epitaxial thin films, colloidal nanocrystals, and organic molecules and polymers. As a result, achieving precise desired emission characteristics may require compromises on emission efficiency and a material's stability. For example, the spectral sharpness of spontaneous emission can be challenging to achieve because of its intrinsic homogeneous broadening and inhomogeneous broadening due to the variation among contributing emitters. The tuning range of the peak emission without changing the optical output level can also be adversely limited. Similarly, the quantum efficiency of an emitter and performance of its resulting LED (external efficiency) might also be severely constrained. This translates to limited levels of optical brightness and, most of the time, a limited optical power output of a light-emitting device, after a certain point, no matter how hard the device is driven. This may thus require the use of increased numbers of emitters (either a thicker film or a wider film area), bringing about other problems, including fabrication challenges and issues of uniformity and aging.

Another constraint of conventional LEDs is related to their radiation pattern, which is determined by the optical materials' properties. The extraction efficiency of the generated photons is therefore inherently limited by the dielectric environment and surface morphology of the LED. In most cases, the emission cone is wider than necessary, resulting in poor photon management and reducing the usable power of the generated light. Further patterning of the emitter film in pixelated LEDs to realize, e.g., displays can introduce additional difficulties, especially for very high pixel densities across large areas. Moreover, in some applications where polarized light is needed, it is challenging to produce it with isotropic emitters [e.g., quantum dots (QDs)] without additional optics. Achieving more complex functions, such as vortex beam generation or rapid emission modulation, is not possible by solely manipulating the emitters.

Metasurfaces can be integrated into LEDs to transform the emitted light wavefront (*20*–*22*) or shape the emission of embedded emitters (*6*, *23*, *24*). These devices are termed "meta-LEDs," where meta-optics concepts are applied as integral parts of the emitters and/or parts of the device structure (*25*, *26*). Their impact can be truly transformative if they can substantially enhance the emission and extraction efficiencies and improve control over the angular and polarization properties of the emitted light. Designers may use a single metasurface aimed at delivering one of these benefits, or adapt multiple structures to achieve multiple benefits in a single device.

For example, a metasurface can be patterned directly on the top or bottom surface of the device (i.e., contact layers) (*27*). In this configuration, the metasurface acts as a far-field wavefront transformer. Figure 3A shows the concept of integrating a metasurface with a collimated LED to manipulate its emission properties. The advantage of this concept is that the patterning of the metasurface does not affect the integrity of the LED structure and thus minimizes the device efficiency degradation. Using this concept, beam bending of gallium phosphide (GaP) LED emission was demonstrated (Fig. 3B) (*21*). Metasurfaces can also be used to enhance the emission extraction efficiency, especially when LEDs are made of high-index materials such as III-V semiconductors. Figure 3, C and D, present a disordered metasurface concept inspired by nature to enhance the performance of a gallium nitride (GaN) LED (*22*). In addition to enhanced light scattering, disordered metasurfaces offer broadband optical response and introduce distinct optical properties through multiple scattering effects. These structures have been extensively studied for various applications from light extraction to energy harvesting (*28*, *29*).

Another approach to integrate metasurfaces into LEDs is by placing them in the near-field of the emitter layers. This involves defining a resonant nanostructure, such as a metasurface interlayer, directly above, below, or within the emitter film. The metasurface can also be filled with emitters by either carefully placing them into the resonance "hot spots" or by covering the entire structure with an emitter film (*23*, *30*). Figure 3E shows an LED configuration where a nanopillar array is patterned into the active layer (i.e., multi–quantum well). In this case, the GaN metasurface modifies the phase of the emitted light by leveraging the collective resonances of the nanopillars. This phase manipulation effectively alters the in-plane momentum of the emitted photons following the grating equation, redirecting them into specific angles, as shown in Fig. 3F. Recently, it was also demonstrated that patterned electrodes can control the Purcell effect in organic light-emitting diodes (meta-OLEDs; Fig. 3, G and H) to deliver high–spectral purity emission without the need for absorbing color filters at a record-high pixel density of ~10^4 pixels per inch (*6*). When incorporating metasurfaces into an emitter layer, the major challenge is achieving uniform charge injection to avoid issues such as current crowding, local heating, increased resistance, higher turn-on bias, voids, and short circuits that may degrade the device's performance.

The presented examples show that the integration of metasurfaces into LEDs offers notable advantages by improving performance and adding functionality. Metasurfaces allow precise control over light emission, enabling tailored spectral and angular properties. This leads to higher efficiency, color purity, and the integration of advanced optical functions such as beam shaping and polarization control.

Lasers

Light amplification by stimulated emission of radiation (laser) devices play a crucial role in modern technologies, forming the foundation for various applications including medical surgeries, communication networks, manufacturing, and scientific research. Metasurface-based lasers can offer distinct advantages over traditional laser designs by precisely controlling the emission properties such as beam profile, directionality, and polarization. In addition, metasurfaces can facilitate ultrafast tuning of laser properties, which is crucial for applications requiring rapid response times, such as in optical switching and sensing technologies. This level of control and flexibility makes metasurface-based lasers incredibly versatile and efficient, marking a substantial advancement in laser technology.

The concept of nanopatterned lasers was first explored in photonic crystals, which were successfully applied to obtain high–quality (Q) factor laser cavities. Both photonic crystal- and metasurface-based lasers exploit the nanoscale periodic structures to control light propagation and amplification. Whereas the traditional photonic crystal approach relies on the photonic bandgap of periodic structures, metasurfaces offer greater control by using collective resonances of meta-atoms in an array. This allows for additional flexibility in engineering both the Q-factor and the emission properties of the laser. For instance, plasmonic metasurfaces, despite their intrinsic ohmic losses, have been effectively used in optically pumped lasing devices thanks to their high-Q band edge modes (*31*). These narrow resonances, referred to as surface lattice resonances, arise from the diffractive coupling of localized surface plasmon

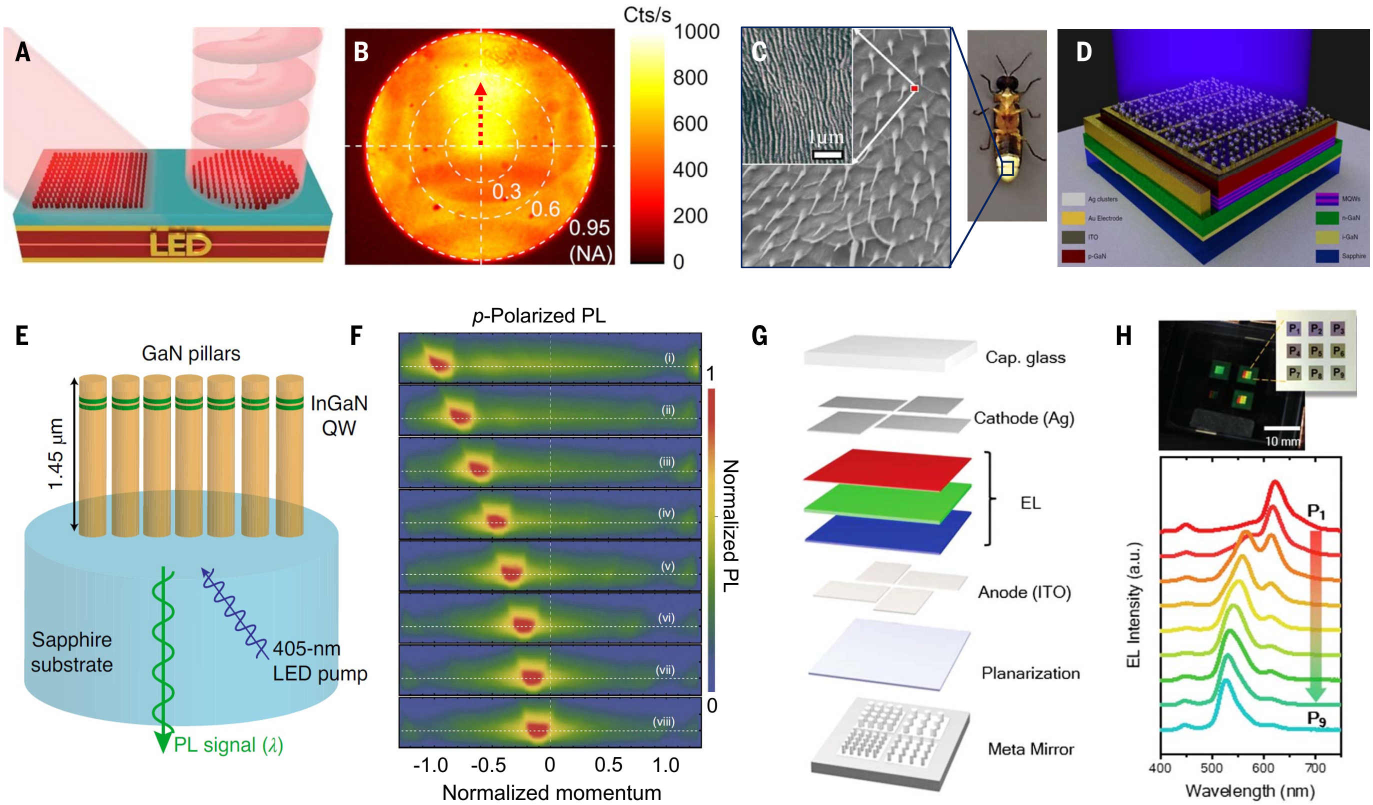

Fig. 3. Metasurface-based LED devices and displays. (**A**) Beam bending and vortex beam generation by integrating a metasurface onto a collimated LED device (*21*). (**B**) Back focal plane image of the photoluminescence (PL) from a GaP meta-LED showing the beam bending effect by the metasurface on top of the LED structure. PL was excited with a 488-nm continuous wave (cw) laser and collected using a microscope objective with numerical aperture (NA) of 0.95 (*21*). (**C**) SEM image of the microstructures on lantern cuticles of *Pyrocoelia rufa* firefly. The inset shows the microstructures at a higher magnification, revealing the disorder in both position and size of stripes (*22*). (**D**) Schematic (not to scale) of a GaN LED with a disordered metasurface patterned on top to enhance light extraction (*22*). (**E**) Illustration of a GaN nanopillar system with embedded InGaN multiple QWs (green) grown on a GaN base layer on a double-sided polished sapphire substrate (*23*). (**F**) p-polarized PL as a function of wavelength (*y* axis, 520 to 580 nm) and normalized in-plane momentum ($k_{||}/k_0$; *x* axis) for the eight different GaN metasurfaces (*23*). (**G**) Cross-section of a meta-OLED with red, green, and blue emitter layers. The different patterns created in the meta-mirror electrode control which colors benefit from a desirable Purcell effect and are effectively emitted from the device (*6*). (**H**) (Upper panel) Photo of a meta-OLED test cell that consists of four sections and is driven at 3 V. The inset shows an optical microscopy image of 3x3 metamirrors with different pitches (P1 to P9). (Lower panel) The electroluminescence from the device shown in (G) where the subwavelength period of the nanopattern is varied from 160 to 380 nm to achieve different emission colors (*6*).

resonances (LSPRs) of individual nanoparticles via evanescent diffraction orders, known as Rayleigh anomalies (RAs). The suppression of the radiative losses and associated high *Q*-factors come from the strong coupling between the RAs and LSPRs, which can be optimized by controlling their detuning. Recently, a way to markedly reduce loss in plasmonic arrays by using nonlocal surface plasmon polaritons (SPPs) was proposed (*32*). The transition from local to nonlocal mode by coupling with diffraction order helps suppress radiative losses and achieve high *Q*. The rise of dielectric resonant nanostructures in recent years with their rich electric and magnetic resonant responses has reignited interest in creating high-finesse optical resonators for lasers with full control over directionality, polarization, and mode profile. Recently, photonic concepts such as the bound state in the continuum (BIC) have been extensively studied and used for lasing devices. Figure 4A shows a directional surface-emitting laser concept by using a periodic array of GaAs nanopillars that support vertical electric dipole resonance (*33*). When these identical dipoles oscillate in phase, the destructive interference leads to the formation of symmetry-protected BIC at the Γ point (i.e., vertical direction). Fundamentally, BICs in periodic photonic lattices are singularities of polarization vortices in the far-field radiation, with the BICs located at the center of the vortex (Γ point in this case). Topological charge of a BIC mode can be determined by the winding number of the polarization vector around the singularity. Lasing emission cannot couple to the singularity point owing to the dark mode nature of BIC but rather couples to a quasi-BIC mode at an oblique angle. By controlling the radiative loss of the quasi-BIC mode via opening leaky diffraction channels, directional lasing can be achieved at desired angles. BICs can also happen at an off-Γ angle (so-called, accidental BIC or Friedrich-Wintgen BIC) when geometrical parameters of the photonic structures are carefully tuned (*34*, *35*). By merging multiple BICs with different topological charges, an even more efficient optical cavity, namely a superBIC, can be created, which has been proven to further lower the lasing threshold (*36*, *37*). Another way to improve the *Q*-factor of BIC cavities with a finite-size array is to use photonic crystal structures with suitable bandgaps at the array boundaries. By using this approach, a *Q*-factor of >10^6 in a BIC cavity with an array size of only ~10 µm by 10 µm has been experimentally demonstrated (*38*). The difference between BIC lasers and traditional surface-emitting lasers (e.g., vertical cavity surface emitting lasers, VCSELs) is that the emitted photons constitute a polarization vortex due to the nonzero topological charge nature of BICs. These polarization states are intrinsically associated with the symmetry of the system. By using a two-beam pumping configuration, ultrafast all-optical switching of a BIC laser mode was achieved with a record

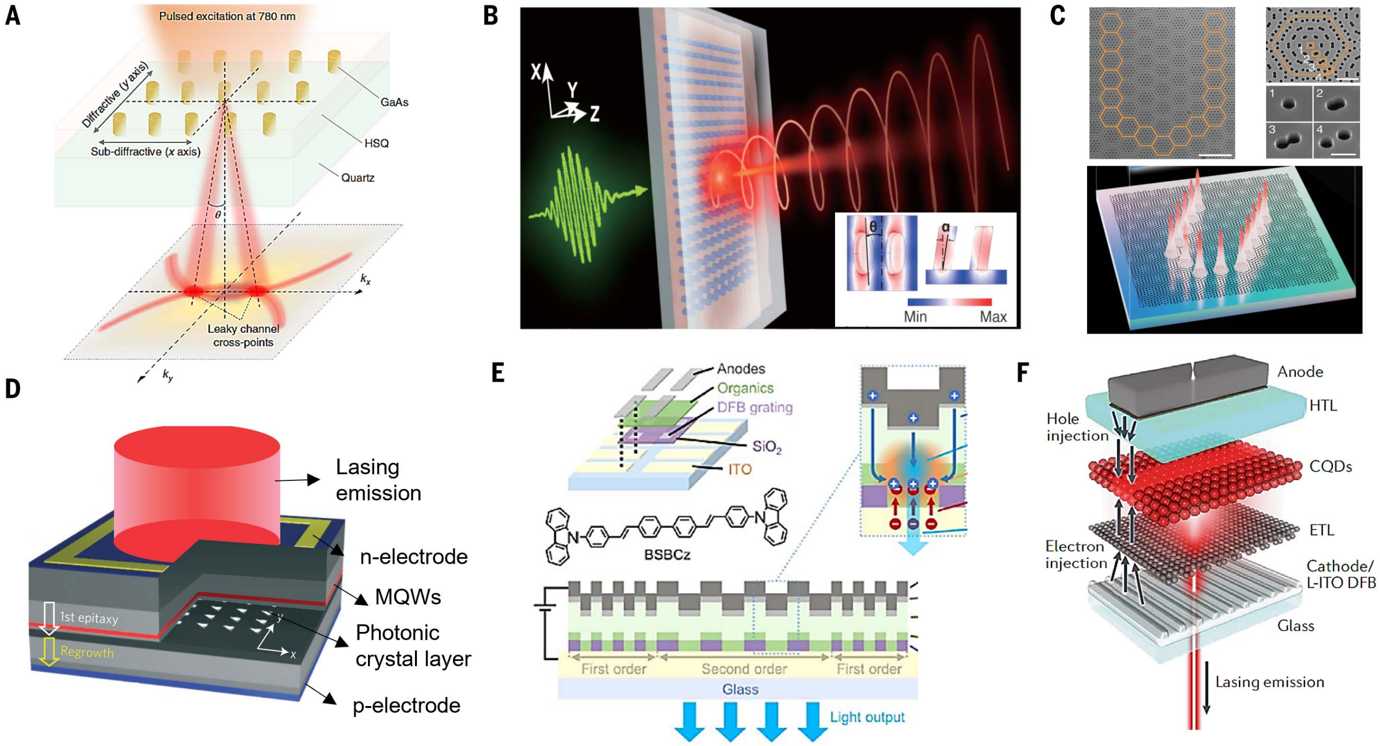

Fig. 4. Metasurface-based lasers. (**A**) Schematics of a GaAs nanopillar array on a fused silica substrate embedded in hydrogen silsesquioxane (HSQ) resist (i.e., spin-on-glass). Along the x axis, the period is fixed at 300 nm (i.e., subdiffractive) to support a symmetry-protected bound state in the continuum (BIC) mode at ~825 nm, while along the y axis, the period P_y is set at 540 nm to create diffractive leaky channels for the directional emission of the laser (*33*). (**B**) Schematic of chiral BIC metasurface made of TiO_2 that can produce chiral lasing with a maximum DOP of 0.98 when coupled with a gain medium such as 2-methyl-6-(4-dimethylaminostyryl)-4H pyran. The chiral BIC mode is formed by doubly breaking geometrical symmetry, as shown in the insets (*40*). (**C**) (Upper panels) SEM images of the U-shaped Moiré nanolaser composed of 17 unit cells of a Moiré superlattice highlighted by orange hexagons. The Moiré superlattice is fabricated in a semiconductor membrane consisting of InGaAsP multiple QWs. Scale bar, 5 μm. (Lower panel) Schematic of a coherent, reconfigurable Moiré nanolaser array that emits U patterns with phase locking (*42*). (**D**) Schematic of the InGaAs-based photonic crystal surface-emitting laser (PCSEL) in which the photonic crystal structure is created by patterning an air-hole array in a p-AlGaAs cladding layer. Arrows indicate the growth direction of the first epitaxial and regrowth structures (*50*). (**E**) Schematic representation of the organic laser diode (OLD) structure using a DFB cavity consisting of SiO_2 nanobeams with widths of 140 and 70 nm for second- and first-order gratings, respectively. Bright, narrow emission, and threshold-like behavior were observed under pulse operation at 50 V. BSBCz: Bis[(N-carbazole) styryl]biphenyl (*52*). (**F**) A proposed quantum dot laser diode (QLD) architecture, which comprises a p-i-n structure assembled on top of a DFB cavity integrated into a lower indium tin oxide (L-ITO) electrode. HTL: hole transport layer; ETL: electron transport layer; CQDs: colloidal quantum dots (*53*).

switching speed and power (*39*). Breaking the symmetry of the nanostructures can also be used to generate lasing emission with circular polarization. Figure 4B shows the TiO_2 nanopillars, specially etched to create tilted structures, which breaks mirror symmetry in the vertical direction. Using this structure, chiral lasing emission was demonstrated with a near-unity degree of polarization (DOP) (*40*). A similar approach was used to demonstrate a chiral metasurface with a high *Q*-factor and circular dichroism by using a TiO_2 slanted hole structure (*41*). In this case, by breaking the symmetry of the nanostructure twice (i.e., in-plane and out-of-plane symmetries), the topological charge of the symmetry-protected BIC can be split and fine-tuned to maximize the purity of the circular polarization. Moiré effects have also been used to demonstrate reconfigurable nanolaser arrays, as shown in Fig. 4C (*42*). The strong localization of the mode within a single unit cell of the Moiré superlattice is induced by a flatband resonance, which is formed when the Moiré twisted angle is carefully tuned. Using this concept and structured pumping technique, various lasing patterns were obtained with high spatial and spectral coherence (*42*). Leveraging the same concept of twisted lattices, the same group has also demonstrated a singular dielectric nanolaser with an ultrasmall mode volume of only ~0.0005 λ^3 (*43*). Other concepts such as Dirac singularity (*44*, *45*), supersymmetry, topological insulator (*46*–*48*), and parity-time symmetry (*49*) have also been used to design new optical cavities for lasers.

Although numerous concepts for the use of resonance nanostructures in lasers have been suggested, their integration into electrically pumped devices remains a challenge. The reason is that the electrical device requirements have not been considered during the photonic design, including the material choice (e.g., conduction band alignment, hole and electron mobility), device architecture (e.g., electrodes, charge injection pathway), and thermal management. In this regard, an optimal photonic design that works well in an optically pumped laser configuration does not necessarily result in a good electrically pumped laser device. To date, there are three main electrically pumped laser device platforms that have been successfully integrated with resonant nanostructures. The first and most efficient one is based on epitaxially grown III-V semiconductors. Here, a resonant nanostructure can be patterned in between epitaxial growth cycles of different device layers as shown in Fig. 4D (*50*). Using this device concept (termed a photonic crystal surface-emitting laser, or PCSEL), a watt-class laser device (*50*), and most recently, continuous-wave single-mode laser (*51*), were demonstrated. The successful integration of resonant nanostructures near the gain medium of PCSEL devices became possible with an innovative regrowth strategy and careful design of photonic nanostructures to ensure an uncompromised electrical performance. The second, long-sought-after lasing platform is based on OLEDs that offer tremendous versatility in their fabrication and benefit from a wide selection of emitting materials to deliver different lasing wavelengths. Figure 4E shows an organic laser diode (OLD) structure having a nanopatterned distributed feedback (DFB) cavity that has been reported to achieve lasing with electrical injection (*52*). The results show that it is possible to achieve high device performance after integrating it with an electrically passive nanostructure made of SiO_2. This opens up the possibility of incorporating resonant nanostructures with new functionalities into such lasing device structures. The third device platform is a quantum dot laser diode (QLD), as shown in Fig. 4F (*53*). QDs made of II-VI semiconductors such as CdSe/CdS can offer several advantages over organic molecules as emitting materials for lasing. They exhibit higher photostability, tunable emission wavelengths through size and composition control, and narrower emission spectra, leading to better lasing performance.

Each device platform has its own challenges when it comes to the integration of resonant nanostructures to form efficient optical cavities without sacrificing electrical performance. For instance, the requirement in lattice mismatch for epitaxial growth in the III-V platform prohibits the use of foreign materials for nanostructures. Etching the whole stack of devices to form resonant nanostructures often results in poor electrical performance. For OLD and QLD, the main issue lies in the low charge injection tolerance of the materials, which is usually below the high current density required for lasing. In addition, owing to the thin-film nature of the devices, any defect due to the integration of resonant nanostructures may result in current crowding and material breakdown. Another important aspect of lasing devices is thermal management during their operation (i.e., at high current density). This is especially important for OLD and QLD where most of the materials constructing the lasers have low thermal conductivity. Addressing all these challenges alongside photonic design aspects is essential for successfully integrating photonic nanostructures into electrically pumped laser devices.

The realization of resonant nanostructure-based laser devices with rich optical functionality will have a substantial impact and applications in various fields such as sensing, optical communication, and quantum technology. Considering the recent progress in nanophotonic design, as mentioned earlier, along with innovative device architectures (*47*, *54*, *55*) and material advancement (*55*, *56*), it is anticipated that the field will mature in the near future.

Optical modulators and switches

Although static metasurfaces have already found their way into multiple optoelectronic applications, the possibility of imparting them with dynamically tunable functionalities has always been a challenge in the metasurface community (*57*–*59*). In particular, making each nanoantenna pixel in the metasurface independently tunable for either phase or amplitude modulation could help to achieve subwavelength dynamic control of optical wavefronts, which is not available within the current technologies. This could open widespread opportunities for applications of such tunable metasurfaces in two-dimensional (2D) and three-dimensional (3D) holographic projectors, augmented and virtual reality (AR/VR) devices, LIDAR for autonomous driving, and more (*60*). To achieve this ambitious goal, metasurfaces will have to be integrated together with electrical circuitry [i.e., complementary metal-oxide-semiconductor (CMOS) electrodes] to drive them at the individual pixel level.

The first studies of electrical switching of metasurfaces have mainly focused on different material platforms, which can provide sufficient tunability to achieve phase (~2π) or amplitude (~1) modulation. Liquid crystals (*61*–*63*), phase-change materials (*64*–*68*), and semiconductors (*69*–*74*) are the most promising platforms from a practical device perspective, each having its own advantages and disadvantages. Other switching mechanisms such as mechanical, thermo-optic, electro-optic, and electrochemical tuning have also been investigated and can be found, e.g., in a recent detailed review (*75*).

Liquid crystals provide high–refractive index changes, low switching voltages (i.e., a few volts), low optical losses in the visible spectrum, and long-term stability after multiple switching cycles. However, they suffer from relatively low switching speeds (>1 ms) and cross-talk between the pixels (*61*–*63*). Phase-change materials also can deliver a high–refractive index change and can keep the changed state without the application of an extra voltage (i.e., nonvolatile switching) but suffer from higher switching voltages required to heat the material and fatigue effects at many switching cycles (*64*–*68*). Electrical gating of semiconductors can be very fast, allowing operation at greater than gigahertz frequencies, but comes with undesirable light absorption and only achieves notable refractive index changes in very thin accumulation, depletion, or quantum-well layers (*69*–*72*). Although there is currently no ideal switching mechanism that can satisfy all requirements at once, one can select a good material platform that is most suitable for a specific application. For example, AR/VR and holographic display applications can benefit from high diffraction efficiencies in the visible spectrum and high cyclability offered by liquid crystals, while being tolerable to their relatively slow (>1 ms) switching speed (*61*, *76*). By contrast, LIDAR devices and communication systems could benefit from the high switching speeds provided by gating semiconductors (*70*), while being less demanding for electrical tunability of the metasurface building blocks. Phase-change materials could be most suitable for reconfigurable static displays or reconfigurable optics where constant cycling of the material is not required. In such applications, the nonvolatile switching, which does not require constant voltage application, could be of great advantage to save energy between rare switching events (*67*).

Another important consideration is the smallest pixel pitch at which the metasurface can be switched without the unwanted cross-talk between neighboring pixels. From an application perspective, it is important to reach a pixel pitch substantially smaller than the existing technology can provide, e.g., a 3.74-μm pixel pitch for liquid crystal on silicon (LCOS) phase-only spatial light modulator (SLM) from Holoeye (*77*). For liquid crystal–based tunable metasurfaces, the individual pixel switching down to a pitch of ~1 μm has been demonstrated (Fig. 5, A to C) (*61*, *63*). The diffraction efficiency of such devices reaches >40%, making them promising for a range of applications, including displays and laser projectors. Further pitch reduction in such tunable metasurfaces is possible but requires dealing with the cross-talk induced within the thin liquid crystal layer as well as the optical interaction between neighboring dielectric nanoantennas. Even smaller pitches of ~500 nm, down to the single nanoantenna level, have been demonstrated for plasmonic metasurfaces based on gating effects, but with a much lower efficiency of a few percent only (*71*). Potential applications of such metasurfaces to LIDAR technology have also been shown (Fig. 5, D and E) (*70*). For phase-change materials, although switching of an individual nanowire and nanoantenna arrays has been demonstrated (*64*–*68*), individual switching of multiple pixels in a metasurface array has not yet been achieved. Here, a thermal cross-talk between the pixels related to the heat-induced switching mechanism should be taken into consideration. Individual pixel control has also been shown, e.g., in plasmonic metasurfaces switched by conducting polymers (*78*–*80*).

The single-pixel tunable metasurface demonstrations mentioned above have only shown 1D arrays of switchable pixels able to produce active beam steering along a single direction. To unleash the full potential of tunable metasurface technologies, however, addressing a 2D array of pixels with individual pixel control is required. The first attempts to do so using conventional single-layer electrode fan-out could only produce small (10 × 10) arrays of 5.2 μm by 5.2 μm pixels (*69*), which is far below what commercial applications require. Transitioning to a larger number of pixels with much smaller sizes would require integration of metasurfaces on top of CMOS circuitry, which can apply different voltages to individual pixels using a control circuit containing transistors beneath each

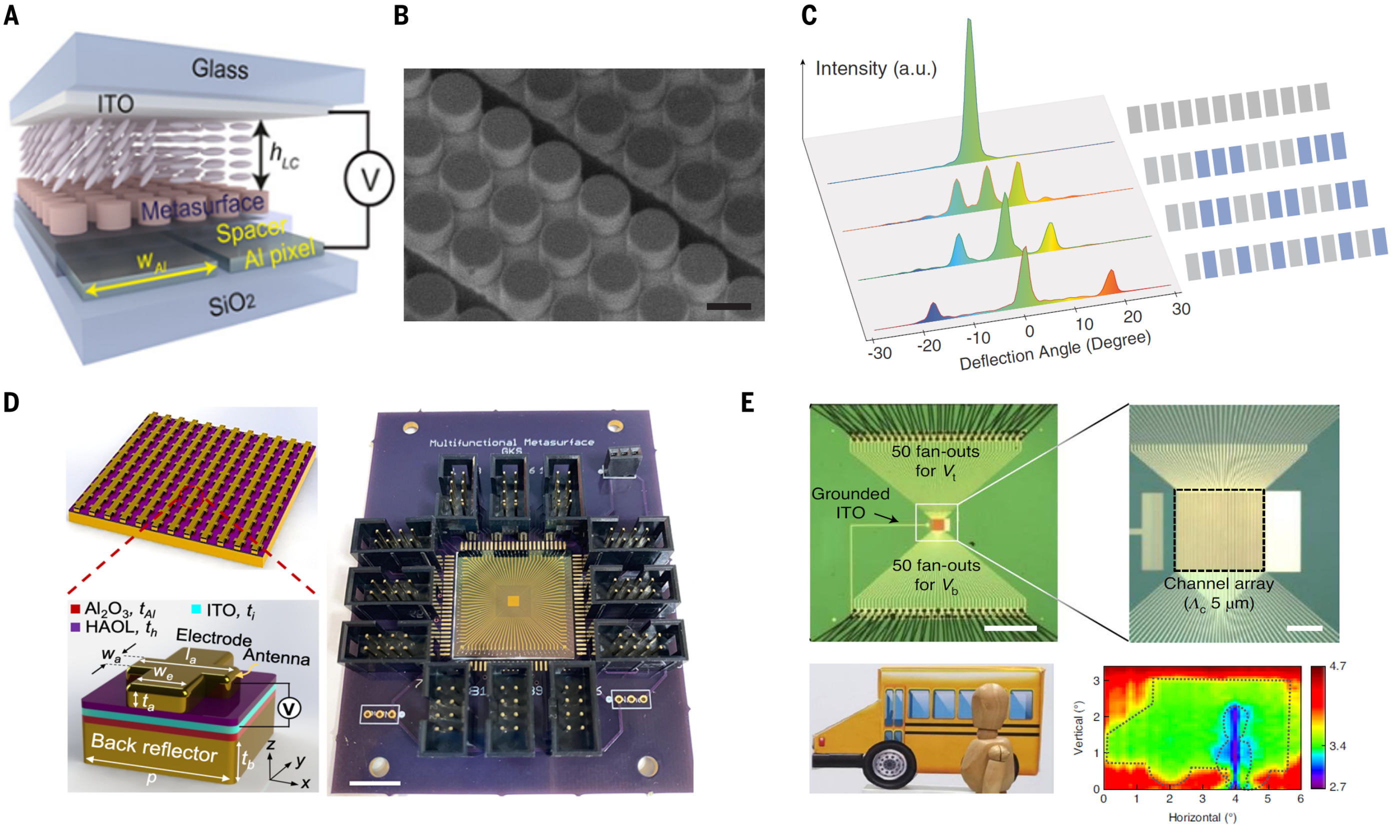

Fig. 5. Examples of tunable metasurface devices and their applications. (**A**) Schematic of a single-pixel tunable reflective metasurface device based on liquid crystals (61). (**B**) Zoomed-in SEM image of 1-μm tunable metasurface pixels with integrated dielectric nanoantennas (63). (**C**) Tunable diffraction grating generated by a transmissive liquid crystal–tunable metasurface with individual pixel control (63). The left side shows the experimentally measured diffraction intensities as a function of the deflection angle for different electrode-addressing configurations, shown on the corresponding right side. Gray patches represent grounded electrodes, and blue patches represent biased ones (at 8 V). a.u: arbitrary units. (**D**) (Left) Schematic of a single-pixel tunable reflective plasmonic metasurface device based on the electrical gating effect. The device consists of an Au back-reflector, an Al_2O_3 dielectric layer, an ITO layer, and a hafnium oxide/aluminum oxide laminated (HAOL) gate dielectric followed by an Au fishbone nanoantenna. (Right) Sample mounting circuit board to control the multifunctional metasurface with 96 individually addressable linear pixels. Scale bar, 10 mm (71). (**E**) (Top) Optical image of the active metasurface array located in the middle of the fan-outs with a size of 250 μm by 250 μm. For the dynamic wavefront manipulation, operating blocks with the period Λ_C of 5 μm were used. Scale bars, 100 μm. (Bottom) A model object for 3D imaging (left) and 3D depth image produced using the metasurface-based SLM (right), which demonstrates the feasibility of the use of the device as the core scanning component in a LIDAR system. The scan angle range, angle step size, and resolution are 6° (H) × 4° (V), 0.2° (H) × 0.2° (V) and 31 × 21 = 651, respectively, where H and V denote the horizontal and vertical axes, respectively (70).

pixel. This, in turn, will impose additional limitations on the maximum voltage, which can be applied to each pixel without destroying the CMOS circuit. A recent presentation showed this kind of integration of a liquid crystal–tunable metasurface on top of a 480 × 640 array (video graphics array resolution) of 1.1 μm by 1.1 μm CMOS pixels (76). With voltages changing in the range of 1 to 2 V, the authors were able to demonstrate dynamic switching of individual pixels, opening the door to realizing 2D dynamic beam steering and tunable 2D holograms with a 100-Hz refresh rate. These results mark a substantial improvement compared to the current state-of-the-art technologies available in industry, showing a strong potential of tunable metasurface devices for practical applications. Further developments in this field are necessary to facilitate commercialization of this technology. This would require simultaneously ensuring multiple factors including low-voltage switching, high diffraction efficiency, fast refresh rates (depending on the application), low power consumption, high uniformity of phase and amplitude modulation across large pixel arrays, and material compatibility with large-volume manufacturing platforms. These are largely associated with engineering and device optimization rather than fundamental issues.

Photodetectors, spectrometers, and imaging systems

The photodetectors found in commercial devices, such as imaging sensors, proximity sensors, and spectrometers, commonly rely on semiconductor p-n junctions, Schottky barriers, or the photoelectric effect to convert optical signals into electrical ones. They are well-suited to measure the light intensity, but all other information carried by the incident photons is typically lost in the photodetection process. Beyond intensity, various properties of light, such as wavelength, phase, polarization, orbital angular momentum (OAM), propagation direction, and spatial and temporal coherence, remain challenging to detect directly with conventional photodetectors without introducing bulky optics. Metasurfaces offer a promising platform to enable the detection of this rich set of properties of light through compact integration of subwavelength meta-atoms with photodetection and imaging systems. With sophisticated design involving geometry, antenna layout, and suitable materials, recent demonstrations of these metasurface-integrated photodetectors (MIPDs) promise a new generation of photodetectors and imaging systems.

In contemporary consumer electronics, a considerable challenge arises from the mismatch between the microscale of optics and the nanoscale of modern electronic devices, resulting in penalties related to power dissipation, area, noise, and latency (81). To address this, an efficient approach involves employing MIPDs to enhance photoelectric conversion efficiency using meta-atoms, thereby improving light harvesting and enabling subwavelength active areas. In alignment with general units in electronics, such as transistors, memory, and logic components, metal nanoantennas can, for example, be combined with doped semiconductors to form Schottky photodiodes and play a dual electronic and optical function. Light from free space can excite plasmons in the metal nanoantenna (82), concentrating the light and enhancing the generation of hot electrons and nanoscale thermoplasmonic effects (83). For example, gold nanoantennas were used to concentrate near-infrared light into a subwavelength germanium photodetector, substantially enhancing its performance (81). The Schottky photodiode can also be simplified using a hybrid silicon-aluminum nanostructure to realize submicrometer pixel dimensions as shown in Fig. 6A (84). The design uses hybrid Mie-plasmon resonances to achieve color-selective light absorption, which is highly localized within the silicon nanocylinders. This localization minimizes the distance between color filters and the photodetector elements, reducing optical crosstalk that typically occurs when light from one filter is absorbed by neighboring photodetectors.

To obtain the spectral information rather than the simple integral of the incident broadband light into a single current value, spectroscopy

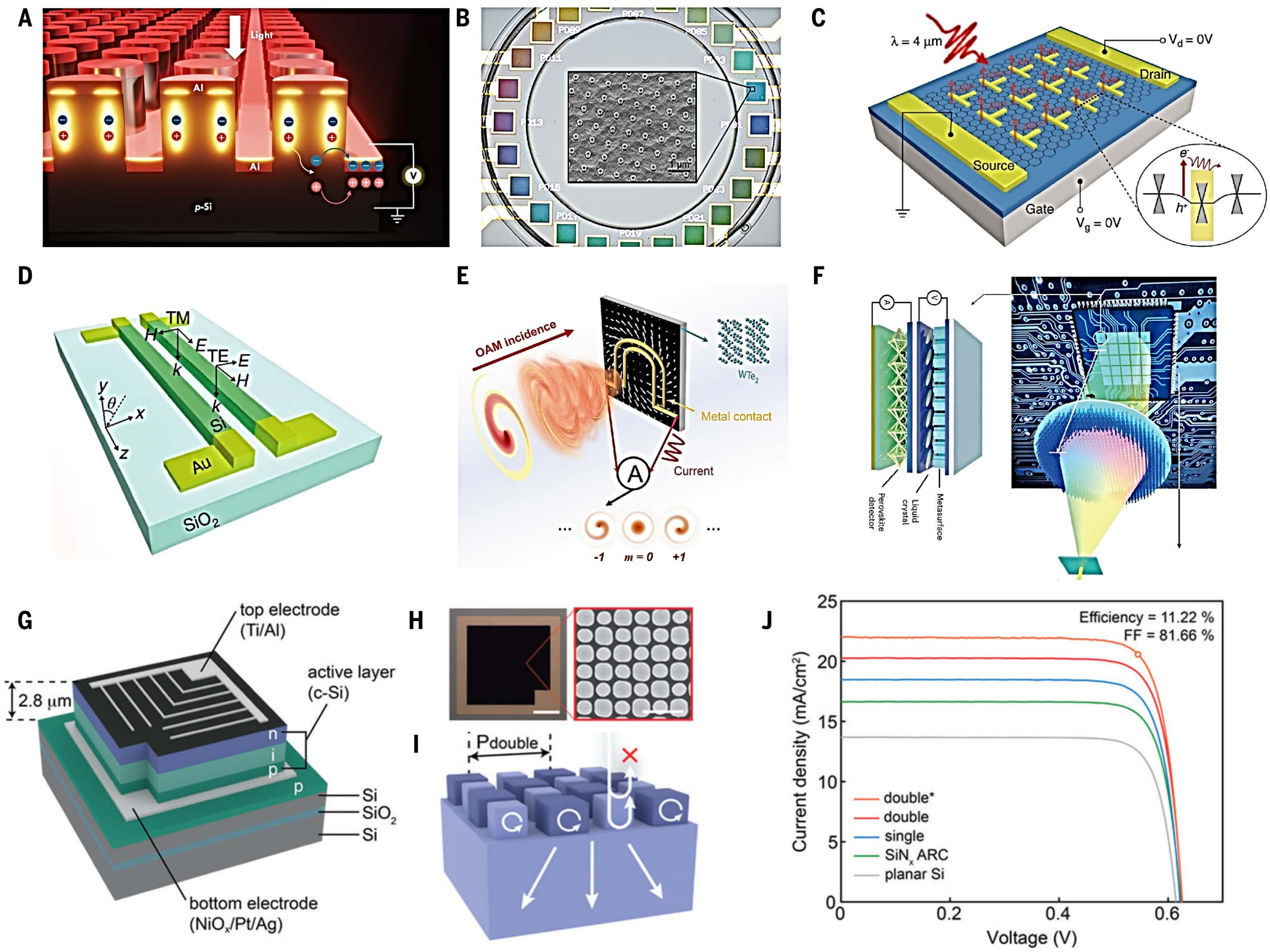

Fig. 6. Metasurface-based photodetectors and solar cells. (**A**) Schematic of the Al-Si hybrid color-selective photodetector (84). (**B**) Photograph of a device mounted in a chip with 24 different structurally colored Si nanowire photodetectors with various diameters for spectral measurement. Inset shows SEM image of one patch of nanowires embedded in the photoresist layer (85). (**C**) Illustration of the graphene-MIPDs consisting of noncentrosymmetric subwavelength metallic nanoantennas on top of graphene flakes. Global directional photocurrent can be generated at zero external bias to mimic the shift current in the bulk photovoltaic effect for polarization detection (92). (**D**) Unit of angle-sensing photodetector with a pair of Si nanowires connected with Au contacts (93). (**E**) Illustration for OAM detection with photocurrent measurement by U-shaped electrodes on WTe_2 (95). (**F**) Compact angle-resolved metasurface spectrometer consisting of liquid crystal–infiltrated metasurface integrated with perovskite photodetectors (96). (**G**) Schematic of an ultrathin solar cell integrated with nanostructured light-trapping antireflection coating (LARC) shown as the dark region in the schematic. (**H**) White-light optical micrograph image (left) and SEM image (right) of the top surface of the c-Si solar cell in (G) that appears dark as a result of the LARC structures. (**I**) A schematic of a LARC structure composed of nanoscale Mie resonators with a bimodal size distribution (**J**) Current–voltage characteristics of 2.8-μm-thick Si solar cells with different types of photon management schemes: a LARC with a bimodal size distribution of Mie resonators (red), a single-sized Mie-resonant ARC (blue), a conventional SiNx ARC (green), and a planar cell without an ARC (gray). The orange curve shows the highest-efficiency cell with a bimodal LARC on a different wafer. Cells with low surface recombination velocities and high efficiencies (η = 11.22%) can be realized, showing the promise of metasurface-based light-trapping strategies. (G to J) Reproduced from (103).

is necessary, typically requiring wavelength selectivity and a detector. Metasurfaces facilitate the construction of ultracompact and lightweight spectrometers with solely detector arrays. For example, structurally colored, doped, vertical silicon nanowire arrays allow the engineering of responsivity spectra in a single chip, combining wavelength selectivity and photodetection functions, as shown in Fig. 6B. This architecture enables spectral reconstruction of an unknown light source based on an algorithm that considers the measured photocurrents from the pixels and a library of their responsivity spectra (*85*). By manipulating the radiative coupling between horizontally arrayed silicon nanowires, imperceptible photodetectors onto transparent substrates can be realized, opening a promising platform for augmented reality, wearables, and sensing applications (*86*). This strategy could overcome the disadvantages of traditional color sensors based on organic dye filters regarding durability, low efficiency, and fabrication complexity. Compact devices for video rate hyperspectral imaging with high-definition spatial and spectral resolution can be further made for portable applications such as food safety, disease diagnosis, remote sensing, environmental monitoring, and artwork analysis (*87*).

In addition to spectral detection, polarization can be easily detected by breaking the fourfold rotational symmetry of meta-atoms using rectangular or elliptical shapes. The incident light with varying polarization states excites distinct resonances, resulting in different absorption and photocurrent values (*88*). Combining engineered chiral plasmonic metasurfaces with semiconductors enables the realization of an ultracompact circularly polarized light detector without additional optical elements (*89*). Full-Stokes detection is achieved by three-port polarimeters comprising on-chip chiral plasmonic MIPDs. By manipulating the spatial distribution of chiral meta-atoms, polarization-resolved absorption information can be converted into corresponding polarization-resolved currents of three ports, facilitating reliable polarization reconstruction (*90*). Recently, it was shown how the incorporation of a metasurface diffraction grating into a machine vision imaging system can enable full-Stokes imaging polarimetry (*91*). As shown in Fig. 6C, an artificial bulk photovoltaic effect can be mimicked to realize cascaded polarization-sensitive photoresponse under uniform illumination with graphene-MIPDs for zero-bias uncooled mid-infrared applications. The vectorial photocurrent enables the detection of polarization angle with a single device regardless of the incident power, and its high responsivity holds great potential for exceeding the Shockley-Queisser limit in efficiency (*92*).

Inspired by natural design, electrically isolated but optically coupled Si nanowires can form a subwavelength photodetection pixel that can measure both the intensity and incident angle of light in a highly accurate fashion (Fig. 6D). This capability arises from the non-Hermitian optical coupling of the Mie resonances supported by the wires that causes measurable differences in the photocurrents from the wires that depend on the incident angle (*93*). With a sophisticated arrangement of the unit, direct wavefront detection becomes possible, offering advantages such as high spatial resolution, robustness, and high speed. This enables unprecedented capabilities such as videoframe recording of high-resolution surface topography (*94*).

Additionally, the property of OAM in light holds great promise for enhancing the bandwidth of optical communication networks. However, direct detection of different OAM modes poses a major challenge, as most existing studies focus primarily on optical intensity–related effects, thereby losing crucial phase information. By combining tungsten ditelluride (WTe_2) with precisely engineered U-shaped electrode geometries (Fig. 6E), it becomes possible to directly characterize the topological charge of the incident OAM beam. The helical phase gradient drives the orbital photogalvanic effect, resulting in a photocurrent that directly reflects different OAM modes. This approach enables the detection of both scalar and vectorial OAM beams, allowing for a determination of the OAM order or the coordinates of any arbitrary OAM state on a higher-order Poincaré sphere. Through photocurrent measurement via a small matrix of electrodes, including arbitrary OAM mixtures, the nonlocal orbital photogalvanic effect holds considerable potential for advancing the development of high-capacity optical chips and next-generation photoelectronic circuits (*95*).

Beyond the functionalities realized with individual units, arranging these single functional units into specific layouts and arrays can also enhance the efficiency and enable direct imaging of various properties of the light field, as shown in Fig. 6F. In addition, through sophisticated integration and codesign with methods such as machine learning or inverse design, multifunctional photodetectors can be achieved in near-field or far-field configurations for applications in spectropolarimeters, angle-resolved spectrometers (*96*), superconducting single-photon spectrometers (*97*), etc. Optical computing with metasurfaces is currently an active area of research, typically captured by imaging the calculated results from the metasurface with a photodetector (*98*). Further development could enable direct optoelectronic conversion, achieving optoelectronic computing fusion for applications such as edge extraction and super-resolution reconstruction. This would allow single-shot real-time decision-making with a meta-imager (*99*), reducing heavy computational demands and energy consumption in machine vision technology, with potential applications in medical devices and autonomous driving systems. (*98*)

It is worth noting that a recent breakthrough of low-dimensional materials (LDMs) in optics and electronics offers new possibilities when combined with MIPDs (*100*). Benefiting from the enhanced absorption with metasurfaces, emerging materials such as boron nitride, graphene, and transition-metal dichalcogenides with band gaps covering a wide spectral range from ultraviolet to terahertz may broaden the applications for weak light detection and flexible and wearable optoelectronics (*101*). These materials lend themselves nicely to metasurface integration, either through directly creating nanostructures in them or by ensuring mode overlap with metasurfaces patterned in other materials. The incorporation of LDMs paves the way for photodetectors driven by electronics toward the "more than Moore's" or "beyond Moore's" era.

Future development of MIPDs includes the exploration of new design methods with different physical principles, selecting suitable materials, including quantum dots and perovskite nanocrystals, for specific band applications with structurally enhanced sensitivity, high signal-to-noise ratios, fast response speeds, stability in various environments, etc. Enhancements in signal extraction, calibration, denoising, and analysis are also essential. The functions powered by metasurfaces can be further improved, such as high-efficiency imaging with color routers, direct photoelectric 3D imaging, and complex amplitude imaging. Beyond the classical domain, MIPDs can potentially be used for photon number count and quantum state detection in the quantum domain (*25*). Considering practical industrial applications, miniaturized MIPDs have considerable potential for portable applications such as consumer electronics, health care, and manufacturing, demanding lightweight, high spectral resolution, sufficient spatial resolution, and fast refresh rates. The fabrication technique should be CMOS compatible, enabling seamless ultracompact planar integration and mass production at low cost. With the key advantages of metasurfaces for ultimate miniaturization, empowering new functionalities to process various properties of light, and the opportunity to tune their properties on demand, it is expected that MIPDs will enable smart vision, foreseeing a revolution in the photoelectric detection and imaging of light with multidimensional information (*102*).

Thin-film solar cells

Solar cells capitalize on the special electronic and optical properties of semiconductors to convert sunlight into clean electrical power. These materials display high refractive indices and a polished semiconductor surface, therefore strongly reflecting light. For this reason, transparent layers of dielectrics or conductive oxides and polymers are applied as antireflection coatings to let the light into the cell. Most cells also use light-trapping structures to redirect incident photons into the plane of the cell to boost absorption. On thicker cells, light trapping is achieved with macroscopic, micrometer-scale structures that can deliver power conversion efficiencies as high as 25% for crystalline silicon (c-Si) cells (*103*), the most widely used photovoltaic technology today. However, substantial research and development are currently aimed at exploring ways to reduce the materials usage, weight, and production cost of solar modules. There is also a drive toward increased flexibility. Thin-film cells from a variety of semiconductor materials may provide a viable pathway toward this goal. If proper light-trapping strategies can be developed, they could enable the realization of ultrahigh-efficiency thin cells at low cost and provide the ultimate solution for utility-scale solar. They can also open new application spaces in robotics, aerospace, transportation, internet of things sensors, and wearable devices (*104*).

The conventional macroscopic surface textures commonly applied on thick crystalline cells are not suited for thin devices particularly when the cell thickness is comparable to or smaller than macroscopic texture size. Here, the implementation of nanostructured light-trapping layers is proving to be more effective. Both plasmonic (*105*–*109*) and Mie-resonant (*110*–*115*) light-trapping layers have been developed. Plasmonic antireflection and light-trapping layers always suffer from some unwanted optical absorption losses in the metal. Despite such losses, structured plasmonic back reflectors have been able to deliver power conversion efficiencies comparable to world records in certain materials systems [e.g., dye-sensitized solar cells (*116*)]. In this case, the light can have one pass through the solar cell before interacting with the lossy metal. In many solar cells, metallic back contacts are used for the extraction of photocurrent, and adding nanopatterns for light trapping can be beneficial.

Mie-resonant structures can be patterned directly on semiconductor layers, and therefore offer similar light-scattering and light-trapping functions but do not suffer from the parasitic losses. Mie-resonant antireflection coatings (ARCs) have already been realized at wafer scale (*110*), and the palette of large-area nanopatterning techniques for metasurfaces is rapidly expanding and includes various soft lithography, immersion lithography, nanoimprint lithography, and advanced semiconductor manufacturing technology approaches (*117*–*122*). In such ARCs, the scattering from the nanostructures can effectively cancel the unwanted reflection from a high-index semiconductor substrate through destructive interference. It was recently shown that the introduction of a bimodal size distribution can be used to create light-trapping ARCs (LARCs) where the resonances in the differently sized elements can work together to achieve both effective antireflection and light-trapping functions across the broad solar spectrum (*112*, *123*). In this application, codesign of the electronic and optical properties is critical. The Mie resonators offer light trapping if properly sized. At the same time a thin, high-quality surface passivation layer is needed for such nanopatterned surfaces through thermal oxidation to achieve high power conversion efficiencies. Figures 6, G to J, show how very thin cells supplied with Mie-resonant LARCs can produce notable power conversion efficiency for few-micrometer-thick cells (e.g., 11.2% for a sub-3-μm-thick c-Si solar cell) (*112*).

Perspective and future outlooks

The direct integration of metasurfaces in optoelectronic devices is poised to deliver transformative advances. As the field evolves, we can anticipate a surge in the development of ultracompact, highly efficient, and multifunctional devices that leverage the distinctive light-manipulating capabilities of metasurfaces (*59*, *124*). However, realizing this potential requires a careful codesign approach in which both the photonic and electronic functionalities are optimized in tandem. Metadevices, which simultaneously demand high photonic performance and efficient electronic operation, present specific challenges that necessitate a balanced consideration of both domains. In particular, metasurfaces integrated into optoelectronic devices must strike a delicate balance between controlling light at the nanoscale and maintaining efficient electronic functionality, such as charge injection, field application, and thermal management. Codesign efforts are essential to ensure that while metasurfaces enhance light manipulation (e.g., beam steering, polarization control, or wavelength selectivity), the electronic aspects of the device are not compromised. The photonic and electronic systems must be designed in harmony, from the layout of the nanoresonators to the configuration of electrodes, to avoid issues such as current crowding, excessive resistance, or unwanted thermal effects.

Moreover, the integration of metasurfaces into optoelectronic devices must consider the choice of materials and device architecture. Metadevices can incorporate a variety of materials, each with notable optical and electronic properties. For instance, although high-index dielectric materials like silicon can achieve strong light–matter interaction through Mie resonances, careful attention must be paid to the material's compatibility with the electronic layers. The overall device configuration, such as the placement of metasurfaces relative to the active layers and electrodes, plays a critical role in optimizing both light manipulation and electronic performance.

To bring these metadevices to commercial fruition, large-scale nanopatterning techniques that are compatible with industrial standards are indispensable. Scalability remains a particular challenge for metasurface technologies. Developing manufacturing processes that can reliably produce large-area metasurfaces with subwavelength precision is critical (*125*–*127*). Techniques such as nanoimprint lithography or photolithography supported by advanced semiconductor manufacturing technologies will need to be adapted and refined for high-throughput production, ensuring that metasurface-integrated devices can meet the demands of industrial applications. Looking ahead, collaborative efforts across disciplines, bridging photonics, electronics, materials science, and manufacturing, will be key to overcoming these challenges. The codesign approach, in particular, will be instrumental in realizing the full potential of metasurface-based optoelectronic devices. Additionally, strong partnerships between academia and industry, where scientists and engineers work together, will be crucial for translating research innovations into commercially viable metadevices. These efforts promise to unlock new possibilities in fields ranging from advanced sensors and imaging systems to next-generation displays, optical computing, and quantum technologies.

REFERENCES AND NOTES

1. G. Wetzstein *et al*., Inference in artificial intelligence with deep optics and photonics. *Nature* **588**, 39–47 (2020). doi: 10.1038/s41586-020-2973-6; pmid: 33268862
2. E. Strubell, A. Ganesh, A. McCallum, Energy and policy considerations for modern deep learning research. *Proceedings of the AAAI Conference on Artificial Intelligence* **34**, 13693–13696 (2020).
3. A. Andrae, Comparison of Several Simplistic High-Level Approaches for Estimating the Global Energy and Electricity Use of ICT Networks and Data Centers, Comparison of Several Simplistic High-Level Approaches for Estimating the Global Energy and Electricity Use of ICT Networks and Data Centers. *Int. J. Green Technol.* **5**, 50–63 (2019). doi: 10.30634/2414-2077.2019.05.06
4. J. A. Schuller *et al*., Plasmonics for extreme light concentration and manipulation. *Nat. Mater.* **9**, 193–204 (2010). doi: 10.1038/nmat2630; pmid: 20168343
5. A. I. Kuznetsov, A. E. Miroshnichenko, M. L. Brongersma, Y. S. Kivshar, B. Luk'yanchuk, Optically resonant dielectric nanostructures. *Science* **354**, aag2472 (2016). doi: 10.1126/science.aag2472; pmid: 27856851
6. W. J. Joo *et al*., Metasurface-driven OLED displays beyond 10,000 pixels per inch. *Science* **370**, 459–463 (2020). doi: 10.1126/science.abc8530; pmid: 33093108
7. M. Esfandyarpour, E. C. Garnett, Y. Cui, M. D. McGehee, M. L. Brongersma, Metamaterial mirrors in optoelectronic devices. *Nat. Nanotechnol.* **9**, 542–547 (2014). doi: 10.1038/nnano.2014.117; pmid: 24952475
8. T. Nikolajsen, K. Leosson, S. I. Bozhevolnyi, Surface plasmon polariton based modulators and switches operating at telecom wavelengths. *Appl. Phys. Lett.* **85**, 5833–5835 (2004). doi: 10.1063/1.1835997
9. Q. Li *et al*., A Purcell-enabled monolayer semiconductor free-space optical modulator. *Nat. Photonics* **17**, 897–903 (2023). doi: 10.1038/s41566-023-01250-9

10. J. C. Prangsma *et al*., Electrically connected resonant optical antennas. *Nano Lett.* **12**, 3915–3919 (2012). doi: 10.1021/nl3007374; pmid: 22800440
11. K. C. Y. Huang *et al*., Antenna electrodes for controlling electroluminescence. *Nat. Commun.* **3**, 1005 (2012). doi: 10.1038/ncomms1985; pmid: 22893129
12. M. Esfandyarpour, A. G. Curto, P. G. Kik, N. Engheta, M. L. Brongersma, Optical emission near a high-impedance mirror. *Nat. Commun.* **9**, 3224 (2018). doi: 10.1038/s41467-018-05505-w; pmid: 30104605
13. A. M. Shaltout, J. Kim, A. Boltasseva, V. M. Shalaev, A. V. Kildishev, Ultrathin and multicolour optical cavities with embedded metasurfaces. *Nat. Commun.* **9**, 2673 (2018). doi: 10.1038/s41467-018-05034-6; pmid: 29991722
14. D. Sievenpiper, L. Zhang, R. F. J. Broas, N. G. Alexopolous, E. Yablonovitch, High-impedance electromagnetic surfaces with a forbidden frequency band. *IEEE Trans. Microw. Theory Tech.* **47**, 2059–2074 (1999). doi: 10.1109/22.798001
15. A. Schwanecke *et al*., Optical magnetic mirrors. *J. Opt. A, Pure Appl. Opt.* **9**, L1–L2 (2007). doi: 10.1088/1464-4258/9/1/L01
16. W. Cai, J. S. White, M. L. Brongersma, Compact, high-speed and power-efficient electrooptic plasmonic modulators. *Nano Lett.* **9**, 4403–4411 (2009). doi: 10.1021/nl902701b; pmid: 19827771
17. L. Cao *et al*., Engineering light absorption in semiconductor nanowire devices. *Nat. Mater.* **8**, 643–647 (2009). doi: 10.1038/nmat2477; pmid: 19578337
18. L. Cao, P. Fan, E. S. Barnard, A. M. Brown, M. L. Brongersma, Tuning the color of silicon nanostructures. *Nano Lett.* **10**, 2649–2654 (2010). doi: 10.1021/nl1013794; pmid: 20507083
19. S. J. Kim, P. Fan, J.-H. Kang, M. L. Brongersma, Creating semiconductor metafilms with designer absorption spectra. *Nat. Commun.* **6**, 7591 (2015). doi: 10.1038/ncomms8591; pmid: 26184335
20. Q. Li *et al*., Metasurface optofluidics for dynamic control of light fields. *Nat. Nanotechnol.* **17**, 1097–1103 (2022). doi: 10.1038/s41565-022-01197-y; pmid: 36163507
21. E. Khaidarov *et al*., Control of LED Emission with Functional Dielectric Metasurfaces. *Laser Photonics Rev.* **14**, 1900235 (2020). doi: 10.1002/lpor.201900235
22. P. Mao *et al*., Single-step-fabricated disordered metasurfaces for enhanced light extraction from LEDs. *Light Sci. Appl.* **10**, 180 (2021). doi: 10.1038/s41377-021-00621-7; pmid: 34489399
23. P. P. Iyer *et al*., Unidirectional luminescence from InGaN/GaN quantum-well metasurfaces. *Nat. Photonics* **14**, 543–548 (2020). doi: 10.1038/s41566-020-0641-x
24. W. T. Chen, A. Y. Zhu, F. Capasso, Flat optics with dispersion-engineered metasurfaces. *Nat. Rev. Mater.* **5**, 604–620 (2020). doi: 10.1038/s41578-020-0203-3
25. A. S. Solntsev, G. S. Agarwal, Y. S. Kivshar, Metasurfaces for quantum photonics. *Nat. Photonics* **15**, 327–336 (2021). doi: 10.1038/s41566-021-00793-z
26. A. Vaskin, R. Kolkowski, A. F. Koenderink, I. Staude, Light-emitting metasurfaces. *Nanophotonics* **8**, 1151–1198 (2019). doi: 10.1515/nanoph-2019-0110
27. J. Yun, H. Hirayama, Investigation of Light-Extraction Efficiency of Flip-Chip AlGaN-Based Deep-Ultraviolet Light-Emitting Diodes Adopting AlGaN Metasurface. *IEEE Photonics J.* **13**, 1–13 (2021). doi: 10.1109/JPHOT.2021.3054914
28. Z. Hu, C. Liu, G. Li, Disordered optical metasurfaces: From light manipulation to energy harvesting. *Adv. Phys. X* **8**, 2234136 (2023). doi: 10.1080/23746149.2023.2234136
29. P. Lalanne *et al*., Disordered optical metasurfaces: basics, design and applications. arXiv:2408.09425 [physics.optics] (2024).
30. P. P. Iyer *et al*., Sub-picosecond steering of ultrafast incoherent emission from semiconductor metasurfaces. *Nat. Photonics* **17**, 588–593 (2023). doi: 10.1038/s41566-023-01172-6
31. W. Zhou *et al*., Lasing action in strongly coupled plasmonic nanocavity arrays. *Nat. Nanotechnol.* **8**, 506–511 (2013). doi: 10.1038/nnano.2013.99; pmid: 23770807
32. Y. Liang, D. P. Tsai, Y. Kivshar, From Local to Nonlocal High-Q Plasmonic Metasurfaces. *Phys. Rev. Lett.* **133**, 053801 (2024). doi: 10.1103/PhysRevLett.133.053801; pmid: 39159090
33. S. T. Ha *et al*., Directional lasing in resonant semiconductor nanoantenna arrays. *Nat. Nanotechnol.* **13**, 1042–1047 (2018). doi: 10.1038/s41565-018-0245-5; pmid: 30127475
34. D. A. Bykov, E. A. Bezus, L. L. Doskolovich, Coupled-wave formalism for bound states in the continuum in guided-mode resonant gratings. *Phys. Rev. A* **99**, 063805 (2019). doi: 10.1103/PhysRevA.99.063805
35. S. T. Ha, R. Paniagua-Domínguez, A. I. Kuznetsov, Room-Temperature Multi-Beam, Multi-Wavelength Bound States in the Continuum Laser. *Adv. Opt. Mater.* **10**, 2200753 (2022). doi: 10.1002/adom.202200753
36. J. Jin *et al*., Topologically enabled ultrahigh-Q guided resonances robust to out-of-plane scattering. *Nature* **574**, 501–504 (2019). doi: 10.1038/s41586-019-1664-7; pmid: 31645728
37. M.-S. Hwang *et al*., Ultralow-threshold laser using super-bound states in the continuum. *Nat. Commun.* **12**, 4135 (2021). doi: 10.1038/s41467-021-24502-0; pmid: 34226557
38. Z. Chen *et al*., Observation of miniaturized bound states in the continuum with ultra-high quality factors. *Sci. Bull.* **67**, 359–366 (2022). doi: 10.1016/j.scib.2021.10.020; pmid: 36546087
39. C. Huang *et al*., Ultrafast control of vortex microlasers. *Science* **367**, 1018–1021 (2020). doi: 10.1126/science.aba4597; pmid: 32108108
40. X. Zhang, Y. Liu, J. Han, Y. Kivshar, Q. Song, Chiral emission from resonant metasurfaces. *Science* **377**, 1215–1218 (2022). doi: 10.1126/science.abq7870; pmid: 36074858
41. Y. Chen *et al*., Observation of intrinsic chiral bound states in the continuum. *Nature* **613**, 474–478 (2023). doi: 10.1038/s41586-022-05467-6; pmid: 36653568
42. H.-Y. Luan, Y.-H. Ouyang, Z.-W. Zhao, W.-Z. Mao, R.-M. Ma, Reconfigurable moiré nanolaser arrays with phase synchronization. *Nature* **624**, 282–288 (2023). doi: 10.1038/s41586-023-06789-9; pmid: 38092911
43. Y.-H. Ouyang, H.-Y. Luan, Z.-W. Zhao, W.-Z. Mao, R.-M. Ma, Singular dielectric nanolaser with atomic-scale field localization. *Nature* **632**, 287–293 (2024). doi: 10.1038/s41586-024-07674-9; pmid: 39020170
44. R. Contractor *et al*., Scalable single-mode surface-emitting laser via open-Dirac singularities. *Nature* **608**, 692–698 (2022). doi: 10.1038/s41586-022-05021-4; pmid: 35768016
45. M. P. Hokmabadi, N. S. Nye, R. El-Ganainy, D. N. Christodoulides, M. Khajavikhan, Supersymmetric laser arrays. *Science* **363**, 623–626 (2019). doi: 10.1126/science.aav5103; pmid: 30733416
46. M. A. Bandres *et al*., Topological insulator laser: Experiments. *Science* **359**, eaar4005 (2018). doi: 10.1126/science.aar4005; pmid: 29420263
47. Y. Zeng *et al*., Electrically pumped topological laser with valley edge modes. *Nature* **578**, 246–250 (2020). doi: 10.1038/s41586-020-1981-x; pmid: 32051601
48. B. Bahari *et al*., Nonreciprocal lasing in topological cavities of arbitrary geometries. *Science* **358**, 636–640 (2017). doi: 10.1126/science.aao4551; pmid: 29025992
49. H. Hodaei, M.-A. Miri, M. Heinrich, D. N. Christodoulides, M. Khajavikhan, Parity-time-symmetric microring lasers. *Science* **346**, 975–978 (2014). doi: 10.1126/science.1258480; pmid: 25414308
50. K. Hirose *et al*., Watt-class high-power, high-beam-quality photonic-crystal lasers. *Nat. Photonics* **8**, 406–411 (2014). doi: 10.1038/nphoton.2014.75
51. M. Yoshida *et al*., High-brightness scalable continuous-wave single-mode photonic-crystal laser. *Nature* **618**, 727–732 (2023). doi: 10.1038/s41586-023-06059-8; pmid: 37316656
52. A. S. D. Sandanayaka *et al*., Indication of current-injection lasing from an organic semiconductor. *Appl. Phys. Express* **12**, 061010 (2019). doi: 10.7567/1882-0786/ab1b90
53. J. Roh, Y.-S. Park, J. Lim, V. I. Klimov, Optically pumped colloidal-quantum-dot lasing in LED-like devices with an integrated optical cavity. *Nat. Commun.* **11**, 271 (2020). doi: 10.1038/s41467-019-14014-3; pmid: 31937771
54. K. Yoshida *et al*., Electrically driven organic laser using integrated OLED pumping. *Nature* **621**, 746–752 (2023). doi: 10.1038/s41586-023-06488-5; pmid: 37758890
55. N. Ahn *et al*., Electrically driven amplified spontaneous emission from colloidal quantum dots. *Nature* **617**, 79–85 (2023). doi: 10.1038/s41586-023-05855-6; pmid: 37138110
56. Y.-S. Park, J. Roh, B. T. Diroll, R. D. Schaller, V. I. Klimov, Colloidal quantum dot lasers. *Nat. Rev. Mater.* **6**, 382–401 (2021). doi: 10.1038/s41578-020-00274-9
57. R. Paniagua-Dominguez, S. T. Ha, A. I. Kuznetsov, Active and Tunable Nanophotonics With Dielectric Nanoantennas. *Proc. IEEE* **108**, 749–771 (2020). doi: 10.1109/JPROC.2019.2943183
58. A. M. Shaltout, V. M. Shalaev, M. L. Brongersma, Spatiotemporal light control with active metasurfaces. *Science* **364**, eaat3100 (2019). doi: 10.1126/science.aat3100; pmid: 31097638
59. A. I. Kuznetsov *et al*., Roadmap for Optical Metasurfaces. *ACS Photonics* **11**, 816–865 (2024). doi: 10.1021/acsphotonics.3c00457; pmid: 38550347
60. P. Thureja *et al*., Toward a universal metasurface for optical imaging, communication, and computation. *Nanophotonics* **11**, 3745–3768 (2022). doi: 10.1515/nanoph-2022-0155
61. P. Moitra *et al*., Electrically Tunable Reflective Metasurfaces with Continuous and Full-Phase Modulation for High-Efficiency Wavefront Control at Visible Frequencies. *ACS Nano* **17**, 16952–16959 (2023). doi: 10.1021/acsnano.3c04071; pmid: 37585264
62. A. Komar *et al*., Electrically tunable all-dielectric optical metasurfaces based on liquid crystals. *Appl. Phys. Lett.* **110**, 071109 (2017). doi: 10.1063/1.4976504
63. S.-Q. Li *et al*., Phase-only transmissive spatial light modulator based on tunable dielectric metasurface. *Science* **364**, 1087–1090 (2019). doi: 10.1126/science.aaw6747; pmid: 31197013
64. Y. Zhang *et al*., Electrically reconfigurable non-volatile metasurface using low-loss optical phase-change material. *Nat. Nanotechnol.* **16**, 661–666 (2021). doi: 10.1038/s41565-021-00881-9; pmid: 33875868
65. S. Abdollahramezani *et al*., Electrically driven reprogrammable phase-change metasurface reaching 80% efficiency. *Nat. Commun.* **13**, 1696 (2022). doi: 10.1038/s41467-022-29374-6; pmid: 35354813
66. Y. Wang *et al*., Electrical tuning of phase-change antennas and metasurfaces. *Nat. Nanotechnol.* **16**, 667–672 (2021). doi: 10.1038/s41565-021-00882-8; pmid: 33875869
67. C. C. Popescu *et al*., Electrically Reconfigurable Phase-Change Transmissive Metasurface. *Adv. Mater.* **36**, e2400627 (2024). doi: 10.1002/adma.202400627; pmid: 38724020
68. Z. Fang *et al*., Nonvolatile Phase-Only Transmissive Spatial Light Modulator with Electrical Addressability of Individual Pixels. *ACS Nano* **18**, 11245–11256 (2024). doi: 10.1021/acsnano.4c00340; pmid: 38639708
69. S. I. Kim *et al*., Two-dimensional beam steering with tunable metasurface in infrared regime. *Nanophotonics* **11**, 2719–2726 (2022). doi: 10.1515/nanoph-2021-0664
70. J. Park *et al*., All-solid-state spatial light modulator with independent phase and amplitude control for three-dimensional LiDAR applications. *Nat. Nanotechnol.* **16**, 69–76 (2021). doi: 10.1038/s41565-020-00787-y; pmid: 33106642
71. G. K. Shirmanesh, R. Sokhoyan, P. C. Wu, H. A. Atwater, Electro-optically Tunable Multifunctional Metasurfaces. *ACS Nano* **14**, 6912–6920 (2020). doi: 10.1021/acsnano.0c01269; pmid: 32352740
72. Y.-W. Huang *et al*., Gate-Tunable Conducting Oxide Metasurfaces. *Nano Lett.* **16**, 5319–5325 (2016). doi: 10.1021/acs.nanolett.6b00555; pmid: 27564012
73. S. Wang *et al*., A broadband achromatic metalens in the visible. *Nat. Nanotechnol.* **13**, 227–232 (2018). doi: 10.1038/s41565-017-0052-4; pmid: 29379204
74. M. L. Tseng *et al*., Vacuum ultraviolet nonlinear metalens. *Sci. Adv.* **8**, eabn5644 (2022). doi: 10.1126/sciadv.abn5644; pmid: 35442736
75. T. Gu, H. J. Kim, C. Rivero-Baleine, J. Hu, Reconfigurable metasurfaces towards commercial success. *Nat. Photonics* **17**, 48–58 (2023). doi: 10.1038/s41566-022-01099-4
76. A. I. Kuznetsov, "Flat optics and nanoantenna spatial light modulators for imaging, LiDAR, and 3D holographic display applications" in *High Contrast Metastructures XIII*, C. J. Chang-Hasnain, W. Zhou, A. Alù, Eds. (SPIE, 2024), p. PC128970E.
77. HOLOEYE Photonics AG, GAEA-2 Spatial Light Modulators, https://holoeye.com/products/spatial-light-modulators/gaea-2-phase-only/.
78. J. Karst *et al*., Electrically switchable metallic polymer nanoantennas. *Science* **374**, 612–616 (2021). doi: 10.1126/science.abj3433; pmid: 34709910
79. Y. Lee, J. Karst, M. Ubl, M. Hentschel, H. Giessen, Dynamic beam control based on electrically switchable nanogratings from conducting polymers. *Nanophotonics* **12**, 2865–2871 (2023). doi: 10.1515/nanoph-2022-0801
80. R. Kaissner *et al*., Electrochemically controlled metasurfaces with high-contrast switching at visible frequencies. *Sci. Adv.* **7**, eabd9450 (2021). doi: 10.1126/sciadv.abd9450; pmid: 33952513
81. L. Tang *et al*., Nanometre-scale germanium photodetector enhanced by a near-infrared dipole antenna. *Nat. Photonics* **2**, 226–229 (2008). doi: 10.1038/nphoton.2008.30
82. M. W. Knight, H. Sobhani, P. Nordlander, N. J. Halas, Photodetection with active optical antennas. *Science* **332**, 702–704 (2011). doi: 10.1126/science.1203056; pmid: 21551059
83. K.-T. Lin, H. Lin, B. Jia, Plasmonic nanostructures in photodetection, energy conversion and beyond.

Nanophotonics **9**, 3135–3163 (2020). doi: 10.1515/nanoph-2020-0104
84. J. Ho *et al*., Miniaturizing color-sensitive photodetectors via hybrid nanoantennas toward submicrometer dimensions. *Sci. Adv.* **8**, eadd3868 (2022). doi: 10.1126/sciadv.add3868; pmid: 36417508
85. J. Meng, J. J. Cadusch, K. B. Crozier, Detector-Only Spectrometer Based on Structurally Colored Silicon Nanowires and a Reconstruction Algorithm. *Nano Lett.* **20**, 320–328 (2020). doi: 10.1021/acs.nanolett.9b03862; pmid: 31829611
86. Q. Li, J. van de Groep, Y. Wang, P. G. Kik, M. L. Brongersma, Transparent multispectral photodetectors mimicking the human visual system. *Nat. Commun.* **10**, 4982 (2019). doi: 10.1038/s41467-019-12899-8; pmid: 31676782
87. M. Yako *et al*., Video-rate hyperspectral camera based on a CMOS-compatible random array of Fabry–Pérot filters. *Nat. Photonics* **17**, 218–223 (2023). doi: 10.1038/s41566-022-01141-5
88. J. Hong *et al*., Nonlocal metasurface for circularly polarized light detection. *Optica* **10**, 134 (2023). doi: 10.1364/OPTICA.468252
89. W. Li *et al*., Circularly polarized light detection with hot electrons in chiral plasmonic metamaterials. *Nat. Commun.* **6**, 8379 (2015). doi: 10.1038/ncomms9379; pmid: 26391292
90. M. Dai *et al*., On-chip mid-infrared photothermoelectric detectors for full-Stokes detection. *Nat. Commun.* **13**, 4560 (2022). doi: 10.1038/s41467-022-32309-w; pmid: 35931776
91. N. A. Rubin *et al*., Imaging polarimetry through metasurface polarization gratings. *Opt. Express* **30**, 9389–9412 (2022). doi: 10.1364/OE.450941; pmid: 35299368
92. J. Wei *et al*., Zero-bias mid-infrared graphene photodetectors with bulk photoresponse and calibration-free polarization detection. *Nat. Commun.* **11**, 6404 (2020). doi: 10.1038/s41467-020-20115-1; pmid: 33335090
93. S. Yi *et al*., Subwavelength angle-sensing photodetectors inspired by directional hearing in small animals. *Nat. Nanotechnol.* **13**, 1143–1147 (2018). doi: 10.1038/s41565-018-0278-9; pmid: 30374161
94. S. Yi *et al*., Angle-based wavefront sensing enabled by the near fields of flat optics. *Nat. Commun.* **12**, 6002 (2021). doi: 10.1038/s41467-021-26169-z; pmid: 34650050
95. Z. Ji *et al*., Photocurrent detection of the orbital angular momentum of light. *Science* **368**, 763–767 (2020). doi: 10.1126/science.aba9192; pmid: 32409474
96. G. Cai *et al*., Compact angle-resolved metasurface spectrometer. *Nat. Mater.* **23**, 71–78 (2024). doi: 10.1038/s41563-023-01710-1; pmid: 37919349
97. R. Cheng *et al*., Broadband on-chip single-photon spectrometer. *Nat. Commun.* **10**, 4104 (2019). doi: 10.1038/s41467-019-12149-x; pmid: 31506440
98. S. Colburn, A. Zhan, A. Majumdar, Metasurface optics for full-color computational imaging. *Sci. Adv.* **4**, eaar2114 (2018). doi: 10.1126/sciadv.aar2114; pmid: 29487913
99. H. Zheng *et al*., Multichannel meta-imagers for accelerating machine vision. *Nat. Nanotechnol.* **19**, 471–478 (2024). doi: 10.1038/s41565-023-01557-2; pmid: 38177276
100. W. Xin *et al*., Low-Dimensional-Materials-Based Photodetectors for Next-Generation Polarized Detection and Imaging. *Adv. Mater.* **36**, e2306772 (2024). doi: 10.1002/adma.202306772; pmid: 37661841
101. M. Chai *et al*., Metamaterials-Based Photoelectric Conversion: From Microwave to Optical Range. *Laser Photonics Rev.* **16**, 2100458 (2022). doi: 10.1002/lpor.202100458
102. D. N. Neshev, A. E. Miroshnichenko, Enabling smart vision with metasurfaces. *Nat. Photonics* **17**, 26–35 (2023). doi: 10.1038/s41566-022-01126-4
103. M. A. Green, The path to 25% silicon solar cell efficiency: History of silicon cell evolution. *Prog. Photovolt. Res. Appl.* **17**, 183–189 (2009). doi: 10.1002/pip.892
104. M. O. Reese *et al*., Increasing markets and decreasing package weight for high-specific-power photovoltaics. *Nat. Energy* **3**, 1002–1012 (2018). doi: 10.1038/s41560-018-0258-1
105. H. A. Atwater, A. Polman, Plasmonics for improved photovoltaic devices. *Nat. Mater.* **9**, 205–213 (2010). doi: 10.1038/nmat2629; pmid: 20168344
106. S. K. Cushing, N. Wu, Progress and Perspectives of Plasmon-Enhanced Solar Energy Conversion. *J. Phys. Chem. Lett.* **7**, 666–675 (2016). doi: 10.1021/acs.jpclett.5b02393; pmid: 26817500
107. D. Derkacs, S. H. Lim, P. Matheu, W. Mar, E. T. Yu, Improved performance of amorphous silicon solar cells via scattering from surface plasmon polaritons in nearby metallic nanoparticles. *Appl. Phys. Lett.* **89**, 093103 (2006). doi: 10.1063/1.2336629
108. V. E. Ferry *et al*., Light trapping in ultrathin plasmonic solar cells. *Opt. Express* **18** (Suppl 2), A237–A245 (2010). doi: 10.1364/OE.18.00A237; pmid: 20588593
109. S. Pillai, K. R. Catchpole, T. Trupke, M. A. Green, Surface plasmon enhanced silicon solar cells. *J. Appl. Phys.* **101**, 093105 (2007). doi: 10.1063/1.2734885
110. P. Spinelli, M. A. Verschuuren, A. Polman, Broadband omnidirectional antireflection coating based on subwavelength surface Mie resonators. *Nat. Commun.* **3**, 692 (2012). doi: 10.1038/ncomms1691; pmid: 22353722
111. E. F. Pecora, A. Cordaro, P. G. Kik, M. L. Brongersma, Broadband Antireflection Coatings Employing Multiresonant Dielectric Metasurfaces. *ACS Photonics* **5**, 4456–4462 (2018). doi: 10.1021/acsphotonics.8b00913
112. N. Lee, M. Xue, J. Hong, J. van de Groep, M. L. Brongersma, Multi-Resonant Mie Resonator Arrays for Broadband Light Trapping in Ultrathin c-Si Solar Cells. *Adv. Mater.* **35**, e2210941 (2023). doi: 10.1002/adma.202210941; pmid: 37129216
113. Z. Y. Wang *et al*., Broadband optical absorption by tunable Mie resonances in silicon nanocone arrays. *Sci. Rep.* **5**, 7810 (2015). doi: 10.1038/srep07810; pmid: 25589290
114. D. Visser, D. Y. Chen, Y. Désières, A. P. Ravishankar, S. Anand, Embossed Mie resonator arrays composed of compacted TiO_2 nanoparticles for broadband anti-reflection in solar cells. *Sci. Rep.* **10**, 12527 (2020). doi: 10.1038/s41598-020-69518-6; pmid: 32719504
115. P. Spinelli, A. Polman, Light Trapping in Thin Crystalline Si Solar Cells Using Surface Mie Scatterers. *IEEE J. Photovolt.* **4**, 554–559 (2014). doi: 10.1109/JPHOTOV.2013.2292744
116. I.-K. Ding *et al*., Plasmonic Dye-Sensitized Solar Cells. *Adv. Energy Mater.* **1**, 52–57 (2011). doi: 10.1002/aenm.201000041
117. N. Kooy, K. Mohamed, L. T. Pin, O. S. Guan, A review of roll-to-roll nanoimprint lithography. *Nanoscale Res. Lett.* **9**, 320 (2014). doi: 10.1186/1556-276X-9-320; pmid: 25024682
118. S. H. Ahn, L. J. Guo, High-Speed Roll-to-Roll Nanoimprint Lithography on Flexible Plastic Substrates. *Adv. Mater.* **20**, 2044–2049 (2008). doi: 10.1002/adma.200702650
119. M. Leitgeb *et al*., Multilength Scale Patterning of Functional Layers by Roll-to-Roll Ultraviolet-Light-Assisted Nanoimprint Lithography. *ACS Nano* **10**, 4926–4941 (2016). doi: 10.1021/acsnano.5b07411; pmid: 27023664
120. J. Kim *et al*., Scalable manufacturing of high-index atomic layer-polymer hybrid metasurfaces for metaphotonics in the visible. *Nat. Mater.* **22**, 474–481 (2023). doi: 10.1038/s41563-023-01485-5; pmid: 36959502
121. C.-L. Wu, C.-K. Sung, P.-H. Yao, C.-H. Chen, Sub-15 nm linewidth gratings using roll-to-roll nanoimprinting and plasma trimming to fabricate flexible wire-grid polarizers with low colour shift. *Nanotechnology* **24**, 265301 (2013). doi: 10.1088/0957-4484/24/26/265301; pmid: 23735852
122. https://www.forbes.com/sites/sabbirrangwala/2023/07/05/metalenz-pioneers-high-volume-semiconductor-foundry-based-lens-manufacturing/?sh=1577001b23bd.
123. A. Cordaro *et al*., Antireflection High-Index Metasurfaces Combining Mie and Fabry-Pérot Resonances. *ACS Photonics* **6**, 453–459 (2019). doi: 10.1021/acsphotonics.8b01406
124. S. A. Schulz, Rupert. F. Oulton *et al*., Roadmap on photonic metasurfaces. *Appl. Phys. Lett.* **124**, 260701 (2024). doi: 10.1063/5.0204694
125. E. Khaidarov *et al*., Large-scale vivid metasurface color printing using advanced 12-in. immersion photolithography. *Sci. Rep.* **12**, 14044 (2022). doi: 10.1038/s41598-022-18259-9; pmid: 35982212
126. N. Li *et al*., Large-area metasurface on CMOS-compatible fabrication platform: Driving flat optics from lab to fab. *Nanophotonics* **9**, 3071–3087 (2020). doi: 10.1515/nanoph-2020-0063
127. C. Park *et al*., High-Throughput Fabrication of Large-Scale Metaholograms via One-step Printing. *Adv. Opt. Mater.* **12**, 2301562 (2024). doi: 10.1002/adom.202301562

ACKNOWLEDGMENTS

Funding: S.T.H, J.K.W.Y, H.V.D, and A.I.K acknowledge the funding support from Singapore MTC-Programmatic grant no. M21J9b0085. J.K.W.Y also acknowledges support from Singapore NRF Investigatorship Award grant no. NRF-NRFI06-2020-0005. H.V.D also acknowledges support from TÜBA-Turkish Academy of Sciences. Q.L. and M.L.B. acknowledge funding from an AFOSR MURI grant (no. FA9550-17-1-0002) and a US Department of Energy grant (no. DE-FG07-ER46426). **Competing interests:** The authors declare that they have no competing interests.

Submitted 8 July 2024; accepted 25 October 2024
10.1126/science.adm7442